ACSNANO

www.acsnano.org

ARTICLE

Sensitizing Tumors to Immune Checkpoint Blockage via STING Agonists Delivered by Tumor-Penetrating Neutrophil Cytopharmaceuticals

Meixi Hao,[‡] Lulu Zhu,[‡] Siyuan Hou, Sijia Chen, Xiuqi Li, Kaiming Li, Nianci Zhu, Shanshan Chen, Lingjing Xue, Caoyun Ju,[*] and Can Zhang[*]

Cite This: *ACS Nano* 2023, 17, 1663−1680

Read Online

ACCESS | Metrics & More | Article Recommendations | Supporting Information

ABSTRACT: Immune checkpoint inhibitors (ICIs) have displayed potential efficacy in triple-negative breast cancer (TNBC) treatment, while only a minority of patients benefit from ICI therapy currently. Although activation of the innate immune stimulator of interferon genes (STING) pathway potentiates antitumor immunity and thus sensitizes tumors to ICIs, the efficient tumor penetration of STING agonists remains critically challenging. Herein, we prepare a tumor-penetrating neotype neutrophil cytopharmaceutical (NEs@STING-Mal-NP) with liposomal STING agonists conjugating on the surface of neutrophils, which is different from the typical neutrophil cytopharmaceutical that loads drugs inside the neutrophils. We show NEs@STING-Mal-NP that inherit the merits of neutrophils including proactive tumor vascular extravasation and tissue penetration significantly boost the tumor penetration of STING agonists. Moreover, the backpacked liposomal STING agonists can be released in response to hyaluronidase rich in the tumor environment, leading to enhanced uptake by tumor-infiltrating immune cells and tumor cells. Thus, NEs@STING-Mal-NP effectively activate the STING pathway and reinvigorate the tumor environment through converting macrophages and neutrophils to antitumor phenotypes, promoting the maturation of dendritic cells, and enhancing the infiltration and tumoricidal ability of T cells. Specifically, this cytopharmaceutical displays a significant inhibition on tumor growth and prolongs the survival of TNBC-bearing mice when combined with ICIs. We demonstrate that neutrophils serve as promising vehicles for delivering STING agonists throughout solid tumors and the developed neutrophil cytopharmaceuticals with backpacked STING agonists exhibit huge potential in boosting the immunotherapy of ICIs.

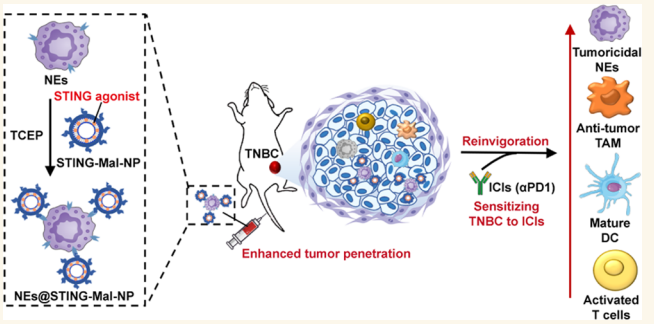

KEYWORDS: *neutrophil cytopharmaceuticals, STING agonists, immune checkpoint inhibitors, tumor penetration, triple negative breast cancer*

INTRODUCTION

Triple-negative breast cancer (TNBC) is characterized by a lack of estrogen receptor (ER), progesterone receptor (PR), and human epidermal growth factor receptor-2 (HER2), which has accounted for approximately 15−20% of breast cancer patients, usually with extremely poor prognosis.[1] Apart from the surgical section, chemotherapy remains the standard therapy of TNBC, but with a disappointing median overall survival of 13−18 months.[2] Inspired by the growing immunotherapy options, immune checkpoint inhibitors (ICIs) such as PD-1/PDL1 antibodies have been attempted to treat TNBC.[3,4] While promising, the responsive rate of ICIs among patients is only 10−35%, which can be primarily attributed to the immunosuppressive tumor microenvironment (TME).[4] The immunologically "cold" TME lacks sufficient T cell infiltration but presents large amounts of immunosuppressive cells that inhibit antitumor immune response,

Received: November 25, 2022
Accepted: December 27, 2022
Published: January 3, 2023

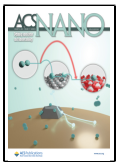

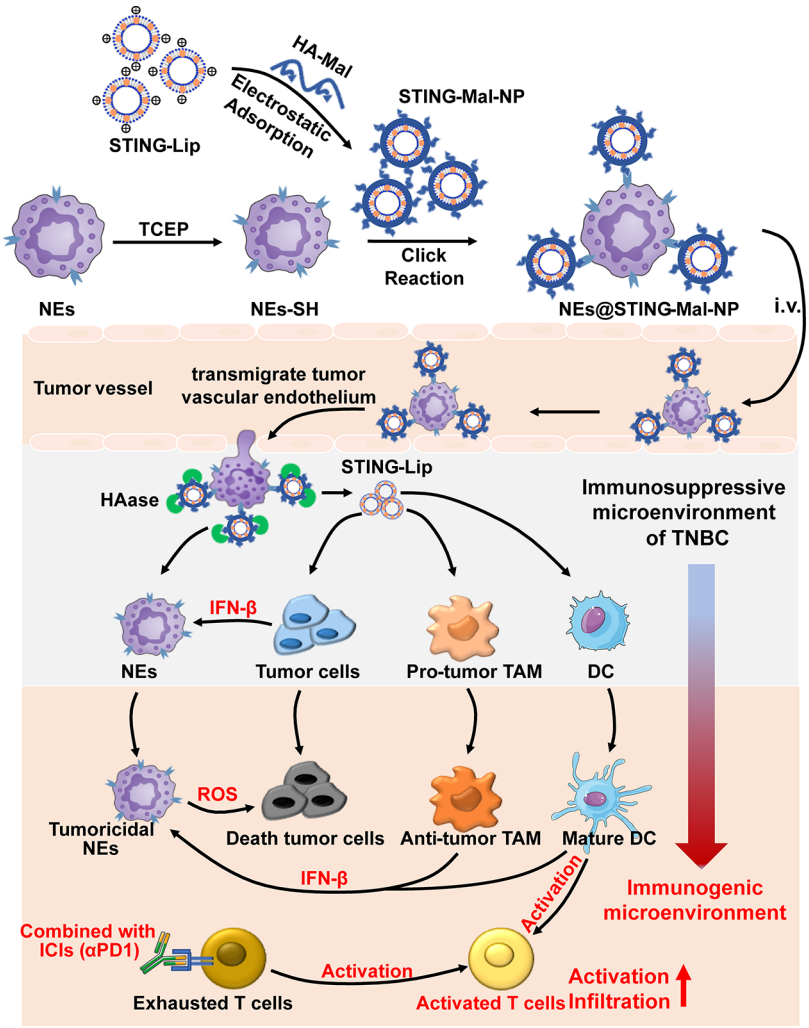

Figure 1. Schematic diagram of tumor-penetrating neutrophil cytopharmaceuticals (NEs@STING-Mal-NP) that enhance the tumor sensitivity and immunotherapy efficiency of ICIs on TNBC. Briefly, NEs@STING-Mal-NP were prepared by the reaction between maleimide on the surface of STING-Mal-NP and thiols on the surface of the NEs-SH (NEs after partial reduction by TCEP). NEs@STING-Mal-NP were endowed with tumor vascular extravasation capacity of NEs to penetrate into the TNBC tumor site. At the tumor site, STING-Lip would be detached from NEs, enhancing the uptake of STING agonist by tumor-infiltrated innate immune cells and tumor cells. The STING signaling was then activated, which reinvigorated immunogenic TME. Finally, the reactivated immunogenic TME by NEs@STING-Mal-NP would sensitize the TNBC tumor to the PD-1 antibody (αPD-1) therapy.

resulting in disabled immunotherapy.[5] Therefore, remodeling the immunosuppressive TME toward immunogenic states would be beneficial for the improved immunotherapy of ICIs in TNBC.[6]

The innate immune stimulator of interferon genes (STING) agonists have been evidenced to reinvigorate the immunogenic TME and sensitize tumors to ICIs.[7,8] As reported, the activation of cyclic guanosine monophosphate-adenosine monophosphate synthase/interferon gene stimulator (cGAS/STING) signaling by STING agonists leads to a multifaceted inflammatory program driven by type I interferon (IFN-I) such as IFN-β.[9−11] It includes directly promoting the apoptosis of tumor cells, recruiting more immune cells, and improving their immune functions, such as enhancing the maturation, activation, and antigen presentation of dendritic cells,[12] regulating the phenotypes of neutrophils and macrophages to tumoricidal ones, and finally boosting the activation of T cells in TME.[13−15] Therefore, the reactivated TME mediated by STING agonists sharply improves the efficacy of ICIs.[16] However, the efficient tumor penetration of STING agonists remains a substantial challenge due to the rapid clearance by the reticuloendothelial system and impeded infiltration by dense tumor extracellular matrix (ECM).[7,17] For example, it is reported that the common delivery carriers of STING agonists such as liposomes, polymer particles, or polymers only lead to 2−10% uptake of STING agonists by tumor-infiltrating innate immune cells or cancer cells.[7,17−20] Moreover, the research group from Massachusetts Institute of Technology recently indicated that carriers with the ability to penetrate tumors can achieve the effective accumulation of STING agonists in tumor sites, resulting in improved cytotoxic T cell priming and long-term tumor remission.[21] Thus, the carriers of STING agonists that can effectively extravasate from the circulation to the throughout tumor tissues plays a central role in aiding robust activation of the STING signaling, thereby ensuring the subsequent antitumor immunity and the boosted efficacy of ICIs.

Neutrophils (NEs) are the largest amounts of leukocytes in peripheral blood with a quick response to inflammation.[22,23] Taking advantage of the inflammatory chemotaxis, our group

https://doi.org/10.1021/acsnano.2c11764
ACS Nano 2023, 17, 1663−1680

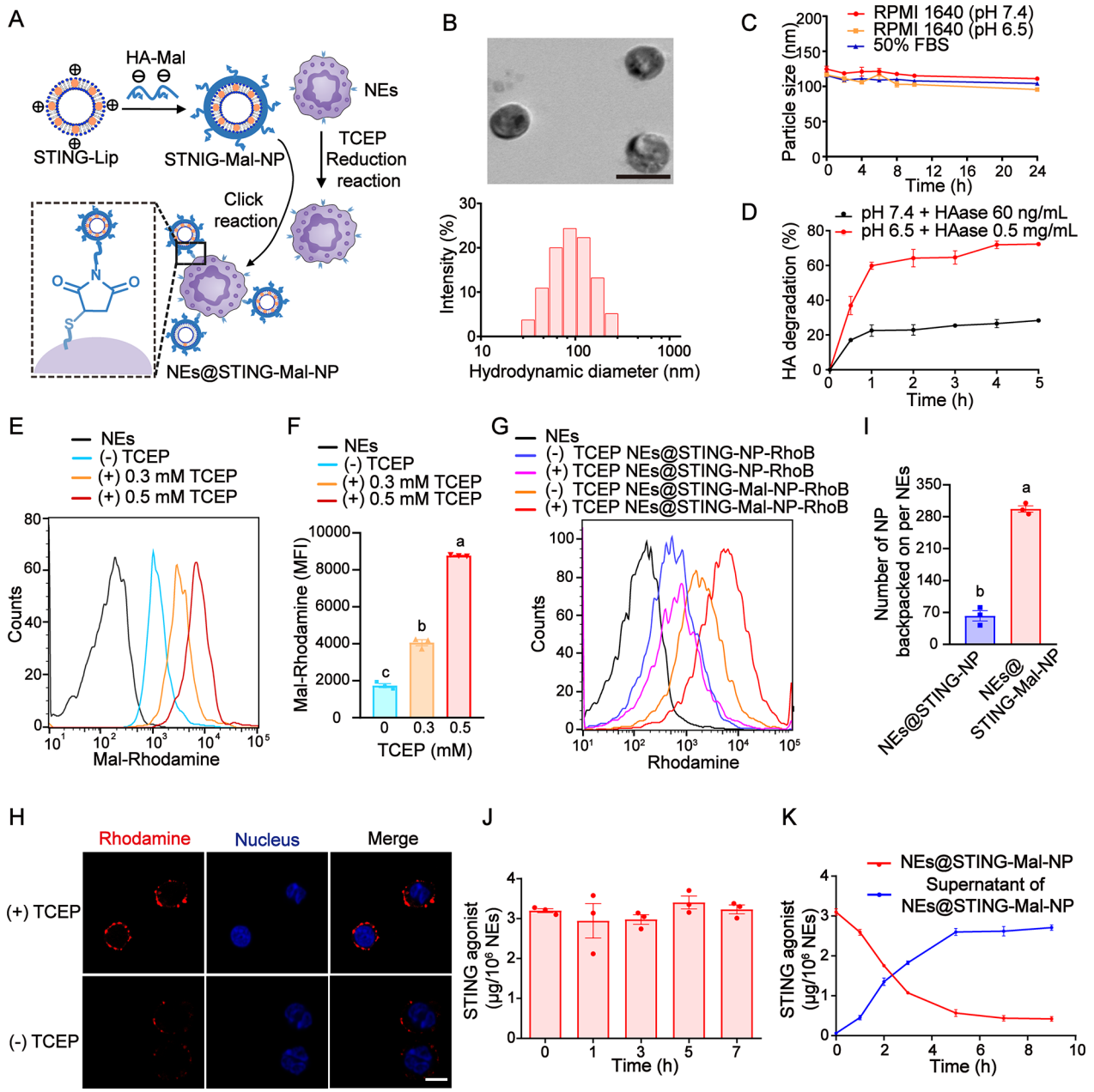

Figure 2. Fabrication and characterization of NEs@STING-Mal-NP. (A) Scheme of NEs@STING-Mal-NP preparation using a reduction-click engineering strategy. (B) Particle size and TEM image of STING-Mal-NP. Bar: 100 nm. (C) Particle sizes of STING-Mal-NP after incubation at different conditions over time. (D) HA degradation of STING-Mal-NP after the incubation with 0.5 mg/mL of HAase at pH 6.5 or 60 ng/mL of HAase at pH 7.4 over time. (E) Flow cytometry analysis and (F) quantification of free thiol levels on NE membrane after the treatment of different concentrations of TCEP. (G) Flow cytometry analysis of NEs with or without TCEP after incubation with STING-NP-RhoB or STING-Mal-NP-RhoB, using NEs as a control. (H) Confocal microscopy images of NEs with or without TCEP after incubation with STING-Mal-NP-RhoB (red). Nucleus was stained by Hoechst 33342 (blue). Scale bar: 5 μm. (I) Number of STING-Mal-NP on the surface of NEs. (J) Amount of STING agonist in NEs@STING-Mal-NP after incubation under 1640 rpmI medium at 37 °C, 5% CO_2 over time. (K) *In vitro* release profiles of STING agonist from NEs@STING-Mal-NP in the presence of HAase (0.5 mg/mL, pH 6.5). Data presented as means ± error bars denote SEM (n = 3). Statistical significance was calculated via one-way ANOVA with Turkey's test (F) and unpaired t test (I). Statistically significant differences were indicated by "abcd", and there are no significant differences between groups marked with the same letter.

has made use of NEs as the drug carriers to load nanomedicines for the fabrication of NE cytopharmaceuticals, which can target the inflammatory site mediated by surgery, hyperthermia, or radiation for treatment of glioma, liver cancer, or gastric cancer with a superior effect than conventional nanoparticles.[24−29] Besides, NEs were also reported to have a capacity of proactive tumor vascular extravasation.[30−32] When sensing the gradient of chemokines, NEs starts to interact with the activated tumor vascular endothelium through the expressions of adhesion molecules, such as L-selectin, P-selectin glycoprotein ligand-1 (PSGL-1), and so on. Subsequently, neutrophils cross the endothelium and tissue barriers through the self-deformation, thus extravasating into the inflammed tissues.[33,34] Moreover, NEs can infiltrated into

https://doi.org/10.1021/acsnano.2c11764
ACS Nano 2023, 17, 1663−1680

the deep tumors owing to their self-deformation ability and survival in hypoxia environment. These merits endow great potential of NEs as drug carriers to penetrate into solid tumors.

Herein, we reported a tumor-penetrating neotype neutrophil cytopharmaceutical, which could leverage the extravasation ability of NEs and release the surface-conjugated liposomal STING agonist in response to the tumor microenvironment. Based on these merits, the neotype neutrophil cytopharmaceuticals hold the capacities of improving the tumor-penetration of STING agonists throughout solid tumors and enhancing the subsequent cellular uptake by tumor-infiltrating cells, leading to effective activation of STING signaling for sensitization tumors to ICIs (Figure 1). Briefly, the tumor-penetrating NE cytopharmaceuticals were prepared to backpack STING agonists onto the cell surface through a reduction-click engineering method,[35] which were different from previously reported NE cytopharmaceuticals with cargos inside the cells.[24] Negative hyaluronic acid-maleimide (HA-Mal)-coated cationic liposomal STING agonists were prepared (STING-Mal-NP) as a backpack. At the same time, NEs were reduced by tris(2-carboxyethyl)phosphine (TCEP) to expose partial free thiols (NEs-SH) for the following conjugation. The facile click reaction then happened to bind the STING agonist-loaded backpack on the surface of NEs through the reaction between maleimide and thiols. The obtained tumor-penetrating NE cytopharmaceuticals (NEs@STING-Mal-NP) inherited the proactive vascular extravasation capacity of NEs, enabling superior tumor penetration. After transmigrating the tumor vascular endothelium and extravasating into the TNBC tumor site, cationic liposomal STING agonists (STING-Lip) would be detached from NEs due to the degradation of HA coating under the hyaluronidase (HAase), enhancing the uptake of STING agonist by tumor-infiltrated innate immune cells and tumor cells. The STING signaling was then activated, which modulated the phenotypes, functions, and potency of tumor-infiltrated innate immune cells, such as neutrophils, macrophages, and dendritic cells, followed by improving T cell-mediated tumor immunity and thus reinvigorating immunogenic TME. The reactivated immunogenic TME by NEs@STING-Mal-NP inspired the tumor sensitivity of ICIs. Overall, NEs appear as a promising vehicle for robust delivery of STING agonists throughout solid tumors, which provide a potent tool in boosting the immunotherapy of ICIs.

RESULTS AND DISCUSSION

Fabrication and Characterization of NEs@STING-Mal-NP. To prove our idea, we first fabricated NEs@STING-Mal-NP as shown in Figure 2A. For preparation of the STING agonist-loaded backpack, cationic liposomes (STING-Lip) loaded with STING agonist-Vadimezan (DMXAA), a classic STING agonist,[36] were prepared by using a film dispersion method. The obtained STING-Lip showed an average particle size of 82 nm and a positive charge of +26 mV, which were then coated with HA-Mal through electrostatic adsorption to gain a HAase-responsive backpack (STING-Mal-NP). When at the optimal C:N molar ratio of 2, STING-Mal-NP displayed an average particle size of 150 nm and a zeta potential of −15 mV (Figure S1), suggesting the stable coating of HA due to the charge conversion from positive to negative. The transmission electron microscopy (TEM) image also indicated the uniform spheroid morphology of STING agonist-loaded backpack (Figure 2B). The drug loading and entrapment efficiency of STING agonist in STING-Mal-NP were measured at 2.8% and 90.4%, respectively. Moreover, we detected the stability and HAase response of STING-Mal-NP. It showed that STING-Mal-NP remained stable *in vitro* within 24 h when incubated under different conditions including physiological conditions (pH 7.4), 50% serum simulated blood conditions, and even in mild acid conditions (pH 6.5, Figure 2C), while in the presence of 0.5 mg/mL HAase at pH 6.5 to mimic the HAase-enriched TNBC tumor microenvironment, the coated HA quickly degraded, and nearly 80% of HA detached from STING-Mal-NP within 8 h (Figure 2D), implying the probable quick release of STING-Lip in the tumor microenvironment.

Afterward, a surface-engineering strategy using a reduction-click reaction was developed to conjugate STING-Mal-NP onto NEs. To provide enough free thiols on the NEs surface for click reaction and without toxicity, different concentrations of TCEP were screened to open the disulfide bonds of membrane protein of NEs. The results showed that the amounts of free thiols increased as the increased concentrations of TCEP and plateaued when the concentration of TCEP reached 0.5 mM (Figure 2E,F). Of note, the concentration of TCEP at 0.5 mM showed no detectable cytotoxicity against NEs (Figure S2A). We further optimized the click reaction conditions including the concentration of STING-Mal-NP and incubation time. To gain the largest drug loading of STING agonist on NEs@STING-Mal-NP while ensuring cell viability, the concentration of STING-Mal-NP was set as 80 μg/mL of STING agonist and the incubation time was 60 min (Figure S2B-D). To further confirm that STING-Mal-NP was conjugated on the cell surface rather than adhesion, rhodamine B-labeled STING agonist-loaded liposomes with HA-Mal coating or with only HA coating were prepared and denoted as STING-Mal-NP-RhoB and STING-NP-RhoB, respectively. NEs with or without TCEP reduction were incubated with STING-Mal-NP-RhoB or STING-NP-RhoB, followed by a flow cytometry assay. As shown in Figure 2G, when NEs were reduced by TCEP incubated with STING-Mal-NP-RhoB, the obtained (+) TCEP NEs@STING-Mal-NP-RhoB displayed the highest fluorescence intensity among other groups, indicating that most of the nanoparticles were on the NEs surface, while the lack of sufficient free thiols or Mal could only achieve modest fluorescence intensity. These results validated that the STING agonist backpacking on NEs was due to click reaction between thiols and Mal rather than physical adhesion. The confocal image also indicated similar results that the STING agonist backpack was conjugated on the surface of NEs due to the TCEP-reduction (Figure 2H). Moreover, we detected about 280 STING-Mal-NP per cell in NE cytopharmaceuticals, whereas there were only 58 STING-NP per cell due to lack of the functional group for the click reaction, indicating that more nanoparticles are conjugated onto the surface of neutrophils than loaded into or adhered onto the cells (Figure 2I). Nearly 3.2 μg of DMXAA was conjugated on the surface per million NEs.

In addition, the stability and release profiles of NEs@STING-Mal-NP under different conditions were evaluated. Under physiological conditions, there was limited STING agonist released from NEs@STING-Mal-NP within 7 h (Figure 2J), while in the mimic HAase-enriched tumor microenvironment, about 70% STING agonist were released due to the degradation of HA coating (Figure 2K). Taken together, we have successfully fabricated the tumor-penetrating NE cytopharmaceuticals backpacking STING agonists, which

https://doi.org/10.1021/acsnano.2c11764
ACS Nano 2023, 17, 1663−1680

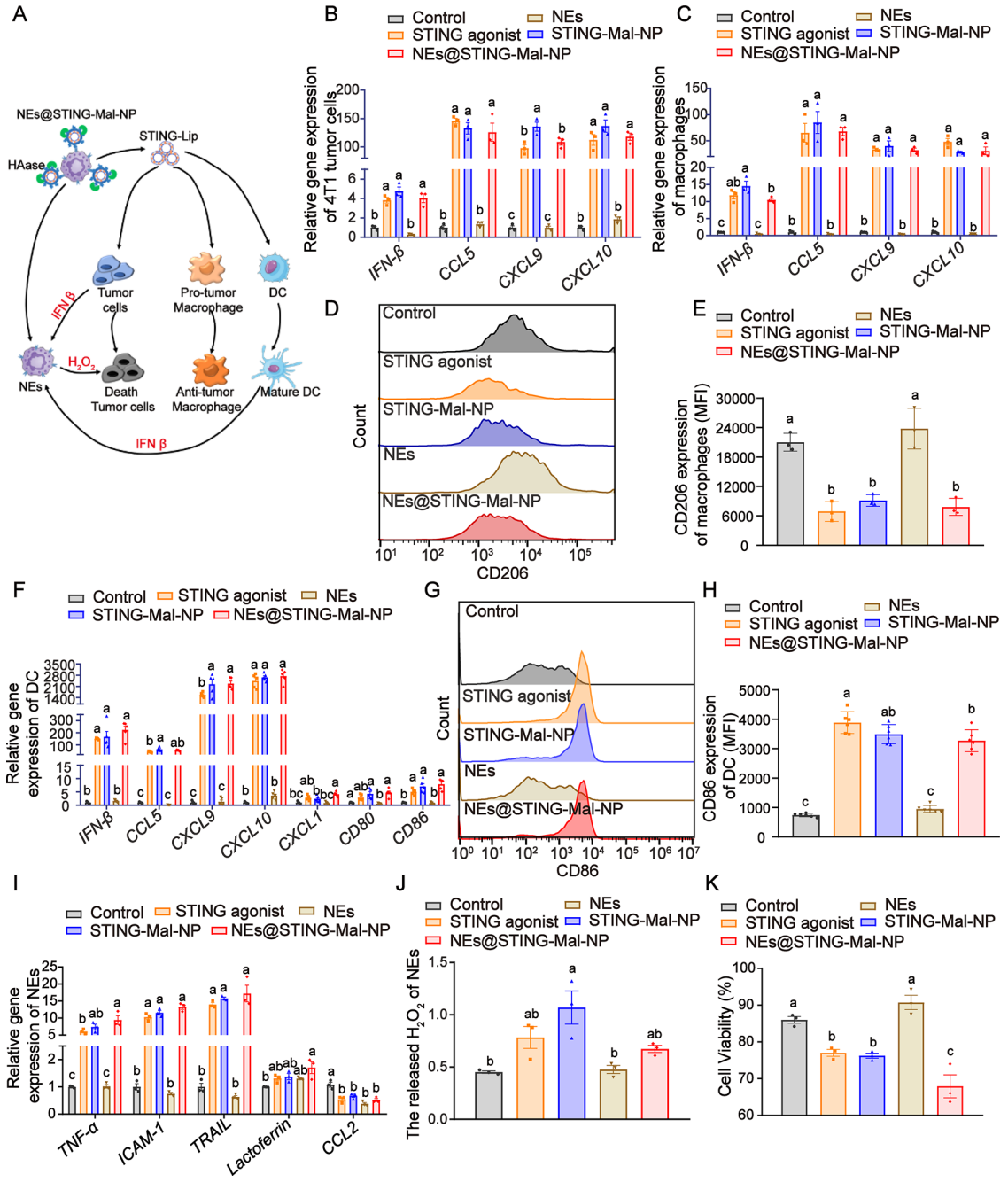

Figure 3. *In vitro* STING signal activation by NEs@STING-Mal-NP. (A) Schematic diagram of activation of STING pathway in tumor cells, macrophages, dendritic cells and NEs via NEs@STING-Mal-NP. (B) Quantitative PCR (qPCR) analysis of STING relative gene expressions including *IFN-β*, *CCL5*, *CXCL9*, and *CXCL10* in 4T1 tumor cells after different treatments (n = 3). (C) qPCR analysis of STING related gene expressions including *IFN-β*, *CCL5*, *CXCL9*, and *CXCL10* in macrophages after different treatments (n = 3). (D) Flow cytometry analysis and (E) quantification of CD206 expression in macrophages after different treatments (n = 3). (F) qPCR analysis of STING relative gene expressions including *IFN-β*, *CCL5*, *CXCL9*, *CXCL10*, *CXCL1*, *CD80*, and *CD86* in dendritic cells (DCs) after different treatments (n = 5). (G) Flow cytometry analysis and (H) quantification of CD86 expression in DCs after different treatments (n = 6). (I) qPCR analysis of STING related gene expressions including *TNF-α*, *ICAM-1*, *TRAIL*, *Lactoferrin*, and *CCL2* in NEs after different treatments (n = 3). (J) Secretion of H_2O_2 from NEs after different treatments, which were activated by PMA (n = 3). (K) Cytotoxicity of NEs after different treatments against 4T1-Luci tumor cells at an effector: target ratio of 10:1 (n = 3). Data presented as means ± error bars denote SEM. Statistical significance was calculated via one-way ANOVA with Turkey's test. Statistically significant differences were indicated by "abcd", and there are no significant differences between groups marked with the same letter.

possess stability *in vitro* and the quick HAase-response in a mimic-tumor microenvironment.

STING Signal Activation Induced by NEs@STING-Mal-NP *In Vitro*. Before investigating the STING signal activation induced by NEs@STING-Mal-NP *in vitro*, we first evaluated whether the surface conjugation affected the viability of NEs. As shown in Figure S3A,B, the apoptosis ratio of NEs@STING-Mal-NP was lower than 10% during 8 h as measured by the cellular apoptosis kit, which showed no significant variations with unconjugated NEs. In addition, trypan blue

https://doi.org/10.1021/acsnano.2c11764
ACS Nano 2023, 17, 1663−1680

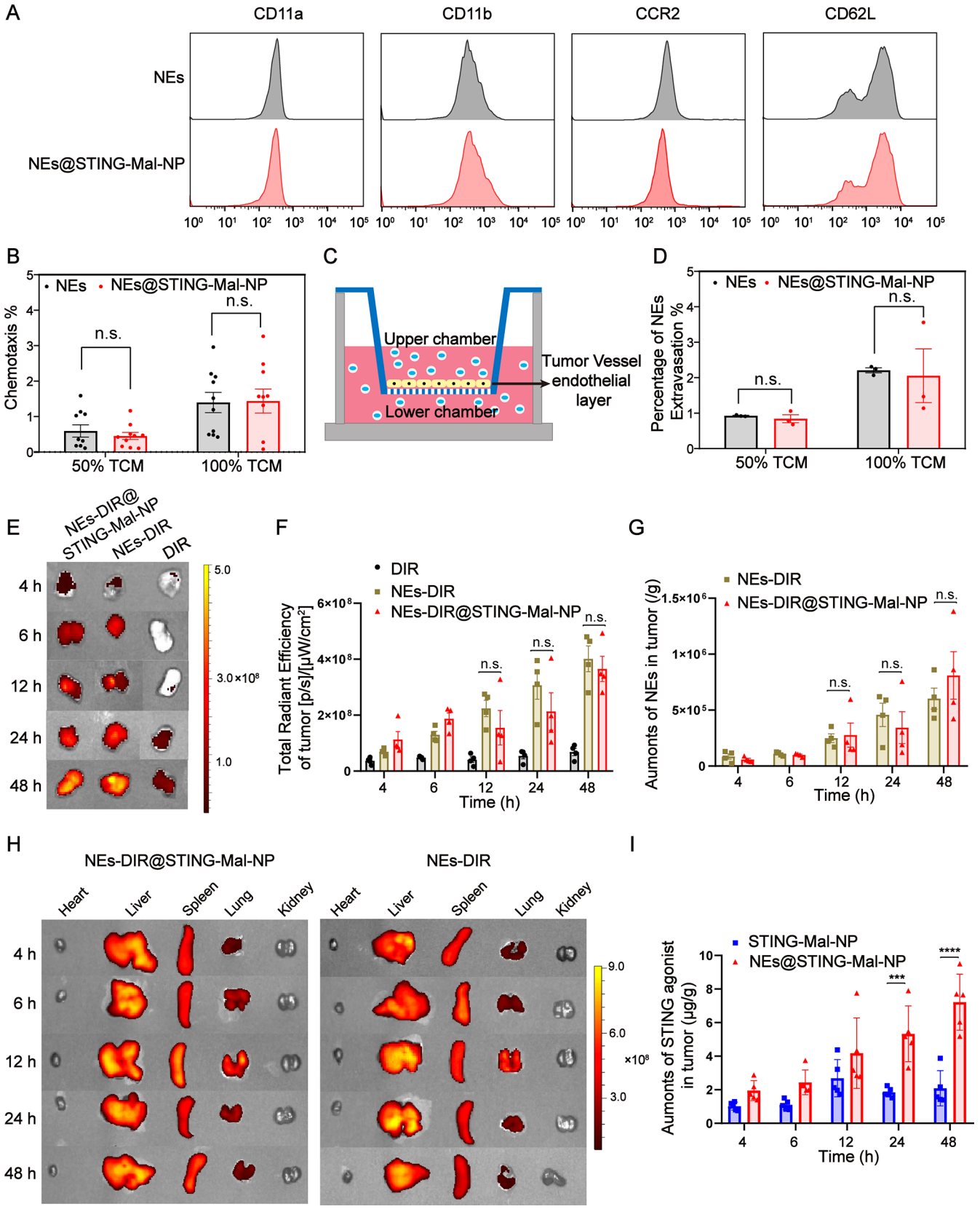

Figure 4. Extravasation and tumor penetration of NEs@STING-Mal-NP. (A) Flow cytometry analysis of the expressions of chemotaxis- and extravasation-related receptors (CCR2, CD62L, CD11a, and CD11b) of NEs@STING-Mal-NP and NEs. (B) Chemotaxis ability of NEs@STING-Mal-NP or NEs under different concentrations of 4T1 TCM (N = 10 fields). (C) Diagram of the transwell assay for exploring the vascular extravasation ability. (D) Vascular extravasation ability of NEs@STING-Mal-NP or NEs under different concentrations of 4T1 TCM (n = 3). (E) *Ex vivo* imaging of DIR in the tumors from 4T1-bearing mice receiving DIR, DIR-NEs, and NEs-DIR@STING-Mal-NP over time. (F) Quantification of DIR fluorescence at (E), n = 4 mice/group. (G) The amounts of DIR-labeled NEs in tumors from 4T1-

https://doi.org/10.1021/acsnano.2c11764
ACS Nano 2023, 17, 1663−1680

Figure 4. continued

bearing mice receiving DIR-NEs, and NEs-DIR@STING-Mal-NP over time by flow cytometry, n = 4 mice/group. (H) Biodistribution evaluation of DIR-NEs and NEs-DIR@STING-Mal-NP in 4T1-bearing mice by using an *ex vivo* imaging system. (I) The amounts of STING agonists in tumors from 4T1-bearing mice receiving STING-Mal-NP and NEs-DIR@STING-Mal-NP over time, n = 5 mice/group. Data presented as means ± error bars denote SEM. Statistical significance was calculated via one-way ANOVA with Turkey's test (F) and unpaired t test (G and I). n.s denotes no significant difference. ***P < 0.001, ****P < 0.0001.

staining analysis displayed that the cell viability of NEs@STING-Mal-NP was above 90% (Figure S3C). These results suggest that the reduction-click engineering process is nondestructive to NEs.

We further performed proteome analysis by Tandem Mass Tag (TMT)-based quantitative proteomics to examine the influence of surface modification on NE proteome and which membrane protein is responsible for the click reaction (Figure S4). Comparing the overall proteome changes between NEs@STING-Mal-NP (without drug loading) and unconjugated NEs, we found that only 21 of 6473 proteins showed more than 1.5-fold change in abundance, suggesting that limited proteins were affected by the reduction-click engineering process. Thereinto, the abundance of most of proteins involved in cell viability, chemotaxis, extravasation, and immune effectors remained unchanged. Of note, we also found that CD45 protein on the surface of NEs offered the mainly thiols, which was consistent with the previous report.[37] This result suggests that STING-Mal-NP can preferably conjugate to specific surface protein rather than the entire pool of proteins displayed on NE surface.

Based on the nondestructive reduction-click engineering, NEs@STING-Mal-NP were expected to release the STING agonist backpack in the TME, followed by endocytosis by various cells, which would subsequently activate the STING signaling pathway (Figure 3A). To prove this, we first measured the STING relative gene expressions including *Interferon β (IFN-β)*, *(C−C motif) ligand 5 (CCL5)*, *(C-X-C motif) ligand 9 (CXCL9)*, and *(C-X-C motif) ligand 10 (CXCL10)*, as well as the protein expression of phospho-STING (p-STING, Ser365) for direct evidence of STING pathway activation in 4T1 tumor cells[38] (Figure 3B and Figure S5). The NEs@STING-Mal-NP group displayed significant up-regulation of the above gene and protein expressions in tumor cells, which was comparable with STING-Mal-NP and free STING agonist, indicating that NEs@STING-Mal-NP could release the backpack in the TME and maintain the immunostimulant effect of STING agonist. In contrast, NEs themselves had no effect on the STING activation in tumor cells. Besides, we found that NEs@STING-Mal-NP could enhance the secretion of STING effector like IFN-β from tumor cells as detected by ELISA assay (Figure S6A). This data further confirmed that NEs@STING-Mal-NP could activate the STING signals in tumor cells.

Afterward, we investigated whether NEs@STING-Mal-NP could activate the STING signaling pathway in macrophages. As shown in Figures 3C, S5, and S6B, significant upregulation of STING-related mRNA levels, p-STING protein expression, and IFN-β secretion induced by NEs@STING-Mal-NP were detected in macrophages. The expressions of *IFN-β*, *CCL5*, *CXCL9*, and *CXCL10* of macrophages after treatment with NEs@STING-Mal-NP were about 13-fold, 56-fold, 45-fold, and 32-fold more than that of untreated macrophages, respectively. To further understand the effect of NEs@STING-Mal-NP on the phenotype of macrophages *in vitro*, the canonical marker of pro-tumor macrophages, mannose receptor (CD206),[39] was detected in interleukin (IL)-4 pretreated macrophages after treatment with different formulations (Figure 3D,E). The expression of CD206 significantly decreased after incubation with NEs@STING-Mal-NP, compared with untreated macrophages, confirming that the phenotype of macrophage converted to the antitumor one via the STING-stimulation of NEs@STING-Mal-NP. Similar effects could be achieved on dendritic cells. After treatment with NEs@STING-Mal-NP, the mRNA levels of STING related mRNA, the p-STING expression, and the secretion of IFN-β from dendritic cells were greatly increased (Figures 3F, S5, and S6C). Moreover, CD86, the mature marker of dendritic cells,[40] was also elevated due to the activation of STING signal that promotes the maturation of dendritic cells (Figure 3G,H).

Apart from these cells, NEs hold low expressions of STING,[41] which indicates that the backpacked STING agonists have limited effect on STING activation of NEs. To prove this, we detected the expression of p-STING in NEs@STING-Mal-NP by Western blot as time over (Figure S7). These results showed that no obvious STING activation could be found in NEs@STING-Mal-NP as compared to NEs. Moreover, the phenotype of NEs in NEs@STING-Mal-NP was analyzed after 12 h of preparation (Figure S8), further indicating that the loaded nanoparticles had no influence on the phenotype change of NEs. However, IFN-β has been reported to act as a negative regulator of the pro-tumorigenic phenotype of NEs.[42] That is, IFN-β might be an effective regulator to modulate NEs as tumoricidal types because we have demonstrated that NEs@STING-Mal-NP could enhance the secretion of IFN-β from tumor cells, macrophages, and dendritic cells. Therefore, we explored the indirect regulation of NEs@STING-Mal-NP on NEs, which were incubated with the cocultured supernatant of NEs@STING-Mal-NP and dendritic cells for 12 h. As expected, antitumor phenotype associated genes such as *tumor necrosis factor-α (TNF-α)*, *intercellular cell adhesion molecule-1 (ICAM-1)*, *TNF-Related Apoptosis Inducing Ligand (TRAIL)*, and *lactoferrin* of NEs were highly upregulated, while the pro-tumor phenotype associated gene like *monocyte chemoattractant protein-1 (CCL2)* was down-regulated (Figure 3I). Next, we evaluated their cytotoxic potency, including hydrogen peroxide (H_2O_2) secretion and cell killing capacity. After phorbol 12-myristate 13-acetate (PMA) activation, the level of H_2O_2 secretion from NEs received indirect regulation by NEs@STING-Mal-NP showed 50% increase than NEs (Figure 3J). Furthermore, NEs@STING-Mal-NP indirect regulation strongly enhanced the cytotoxicity of NEs against luciferase-transfected tumor cells about 20% more than control group at an effector:target ratio of 10:1 (Figure 3K).

Collectively, NEs@STING-Mal-NP exhibit a robust STING activation in TNBC tumor cells, macrophages, and dendritic cells, leading to the increased excretion of IFN-β, the phenotype conversion of macrophages to antitumor type,

https://doi.org/10.1021/acsnano.2c11764
ACS Nano 2023, 17, 1663−1680

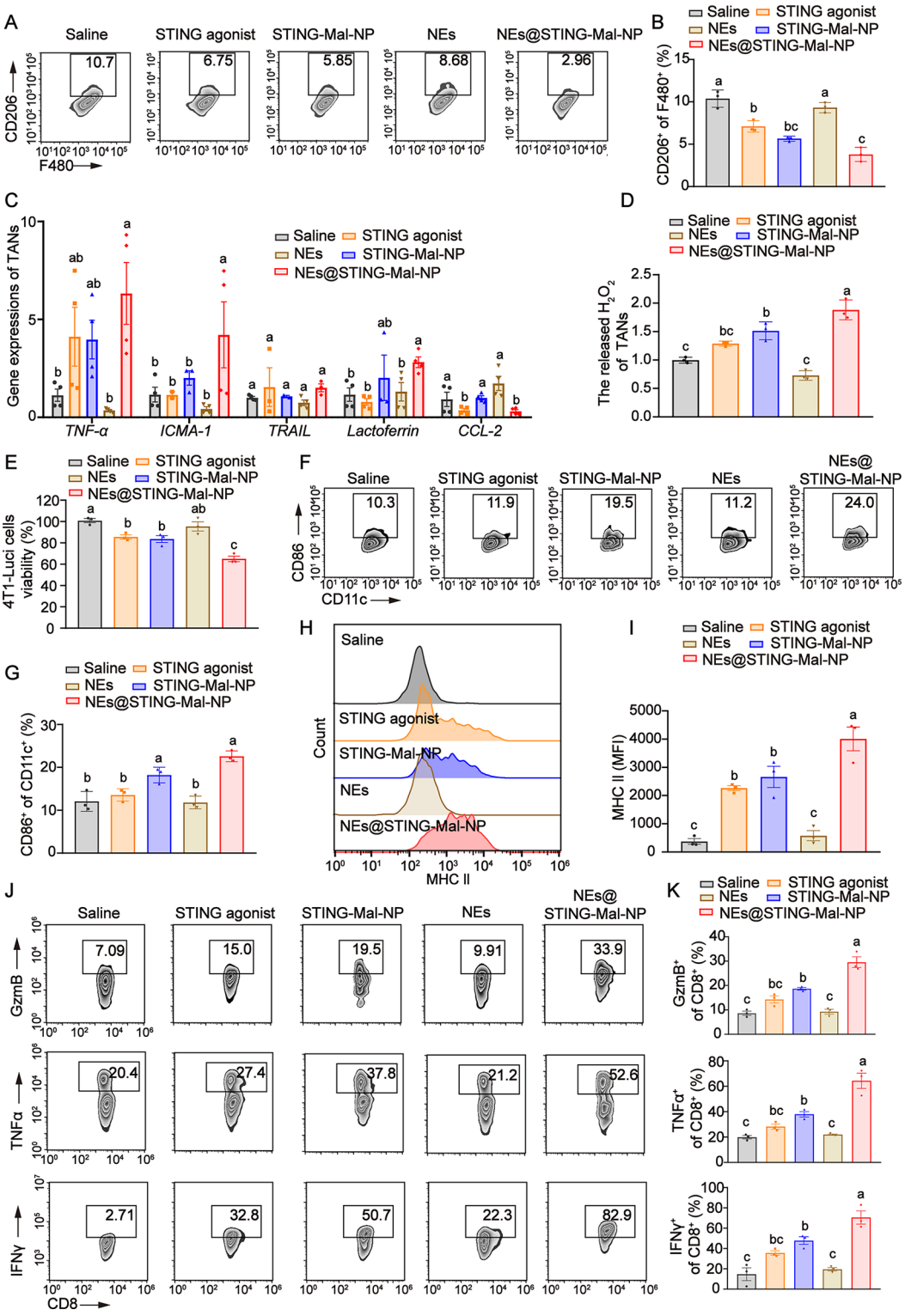

Figure 5. Reinvigoration of the TNBC tumor microenvironment through NEs@STING-Mal-NP. (A) Flow cytometry analysis and (B) quantification of CD206 expression in TAMs isolated from orthotopic 4T1-bearing mice after treatment (n = 3). (C) qPCR analysis of STING related gene expressions including *TNFα*, *ICAM-1*, *TRAIL*, *lactoferrin*, and *CCL2* in TANs isolated from orthotopic 4T1-bearing mice after treatment (n = 4). (D) Quantification of the release of H_2O_2 from TANs after the stimulation with the PMA (n = 3). (E) Evaluation of the killing ability of TANs against 4T1-luci cells (n = 3). (F) Flow cytometry analysis and (G) quantification of CD86 expression of DCs isolated from orthotopic 4T1-bearing mice after treatment (n = 3). (H) Flow cytometry analysis and (I) quantification of MHC II expression of DCs isolated from orthotopic 4T1-bearing mice after treatment (n = 3). (J) Intracellular GzmB, TNFα, and IFNγ in tumor-infiltrating $CD8^+$T cells harvested from isolated from orthotopic 4T1-bearing mice after treatment by using flow cytometry. (K) Quantification of (J), n = 3. Data presented as means ± error bars denote SEM. Statistical significance was calculated via one-way ANOVA with Turkey's test. Statistically significant differences were indicated by "abcd", and there are no significant differences between groups marked with the same letter.

https://doi.org/10.1021/acsnano.2c11764
ACS Nano 2023, 17, 1663−1680

and the mature of dendritic cells. Besides, the excreted IFN-β can further modulate the phenotype of NEs to tumoricidal ones. These results imply the potential of NEs@STING-Mal-NP in remodeling the TME.

Extravasation and Tumor Penetration of NEs@STING-Mal-NP. It has been reported that the tumor penetration of NEs depends on the tumor chemotaxis and vascular extravasation capability of NEs, which were closely associated with their membrane proteins such as chemokine receptors 2 (CCR2), L-Selectin (CD62L), CD11a, and CD11b.[43] Therefore, we detected the levels of CCR2, CD62L, CD11a, and CD11b of NEs@STING-Mal-NP, which displayed no significant changes compared to unconjugated NEs (Figure 4A). This result was consistent to the membrane protein proteome analysis that the abundance of most of proteins involved in cell chemotaxis and extravasation remained unchanged (Figure S4).

Additionally, CD45 protein, an associated protein with the chemotaxis of NEs,[44,45] had been shown to provide the thiol group for conjugation of liposomal STING agonists in NEs@STING-Mal-NP. However, whether the occupation of CD45 protein affected the tumor chemotaxis and vascular extravasation capability of NEs@STING-Mal-NP remained unclear. We thus explored these abilities of NEs@STING-Mal-NP *in vitro* by using the 4T1 tumor cells medium (TCM) as the simulation of TNBC microenvironment. The chemotaxis results showed that NEs@STING-Mal-NP and NEs displayed the similar chemotaxis ability (2.1% vs 2.3%) in a TCM-concentration-dependent manner (Figure 4B). In contrast, the tumor vascular extravasation capacity of NEs@STING-Mal-NP was evaluated by utilizing a transwell assay with human umbilical vein endothelial cell (HUVEC) monolayer, whose transepithelial electrical resistance (TEER) value was over 300 Ω cm^{-2} (Figure 4C). As presented in Figure 4D, the tumor vascular extravasation capacity of NEs@STING-Mal-NP and NEs in response to different concentrations of TCM was also comparable. These results confirmed that the partial occupation of CD45 protein would not influence the chemotaxis and vascular extravasation capacities of NEs@STING-Mal-NP and also indicated the tumor-penetration ability of NEs@STING-Mal-NP inherited from NEs.

The *in vivo* tumor penetration of NEs@STING-Mal-NP was evaluated on orthotopic TNBC tumor-bearing mice via the injection of 4T1-Luci cells into the fourth breast pad of BALB/c mice. We first performed chlorin e6 as a model drug with fluorescence for *in vivo* imaging (Figure S9A−C). After intravenous administration of NEs@Ce6-Mal-NP for 4 h, a Ce6 signal was clearly observed in tumor site. As time over, a stronger Ce6 signal could be monitored and peaked at 12 h. At 48 h, the obvious Ce6 signal of NEs@Ce6-Mal-NP still presented in the tumor site, whereas that of Ce6 and Ce6-Mal-NP gradually diminished (Figure S9D), indicating the excellent tumor penetration of NEs@STING-Mal-NP in orthotopic TNBC.

To better understand the tumor penetration of NE cytopharmaceuticals, we analyzed the biodistribution of NEs-DIR@STING-Mal-NP with NEs labeled by DIR (a near-infrared cell membrane dye), including detection of STING agonist by high performance liquid chromatography (HPLC) and DIR-labeled NEs (NEs-DIR) by *ex vivo* imaging system and flow cytometry (Figure 4E−I, Figures S10 and S11). We found that the infused NEs-DIR@STING-Mal-NP with both NEs as carriers and loaded STING agonist could effectively accumulate at tumor site since 4 h after injection, which was similar to the results observed by Ce6. Of which, the carrier NEs of NEs-NIR@STING-Mal-NP showed the similar tendency with unconjugated NEs, further verifying that the surface-anchoring process had no effect on the chemotaxis of NEs to tumors (Figure 4E,F). Especially, there were about 9×10^5 reinfused NEs in per gram tumor tissues at 48 h after injection detected by flow cytometry, and we calculated that about 19.26% of infused NEs-NIR@STING-Mal-NP accumulated at the tumor site after injection for 48 h (Figure 4G). The DIR fluorescence intensity of the main organs as well as blood was also observed by the *ex vivo* imaging system and quantified by ROI analysis (Figure 4H and Figure S10). The results showed that NEs-DIR@STING-Mal-NP and NEs-DIR were mainly distributed in blood, liver, spleen, and lung after reinfusion, which could be ascribed to the homing ability of NEs to liver and spleen and the retention in lung tissues, confirming the surface-anchoring process would not influence the *in vivo* distribution of neutrophils. Meanwhile, we found that the amount of STING agonist of tumor site at 48 h in the group of NEs-DIR@STING-Mal-NP significantly enhanced to 3.5-fold than that of STING-Mal-NP (Figure 4I). The accumulated ratio of STING agonist at the tumor site was calculated to be 23.2% of the injection dose, demonstrating a dramatic improvement in the accumulation of STING agonist at tumor site due to the tumor-penetrating NE cytopharmaceuticals. In addition, normal tissues such as liver, spleen, and lung also held the STING agonist (Figure S11) due to the biodistribution of NEs (Figure 4H), implying the stably retention of STING-Mal-NP on NEs *in vivo*.

Taken together, NEs@STING-Mal-NP based on the reduction-click engineering inherit the tumor chemotaxis and vascular extravasation capabilities of NEs, which can successfully transmigrate the tumor vascular endothelium and extravasate into the tumor tissues, finally achieving the improved tumor penetration of STING agonist.

Reinvigoration of the TNBC Microenvironment via NEs@STING-Mal-NP. Despite the evidenced excellent tumor penetration of STING agonist via NEs@STING-Mal-NP, the *in vivo* TME reinvigoration mediated by NEs@STING-Mal-NP is still indefinable. We first explored the activation of STING signal pathway in the whole TME. The results showed that the gene expressions of *IFN-β*, *CCL5*, *CXCL1*, *CXCL10*, and *CXCL9* which could recruit and activate immune cells were substantially increased in tumors collected from NEs@STING-Mal-NP-treated mice (Figure S12). Moreover, the dramatically increased numbers of macrophages, dendritic cells, NEs, and CD8$^+$T cells were found in the tumor from NEs@STING-Mal-NP group, compared to other groups (Figures S13 and S14). The gating strategy of Figure S13 is presented in Figure S15A−C.

To understand the improved tumor-infiltrated immune cells in TME, tumor-associated macrophages (TAMs), tumor-associated neutrophils (TANs), tumor-infiltrating dendritic cells, and tumor-infiltrating CD8$^+$ cells were isolated from tumors of 4T1-bearing mice. As displayed in Figure 5A,B, the CD206 positive TAMs were significantly decreased in NEs@STING-Mal-NP-treated mice, indicating that NEs@STING-Mal-NP mediated repolarization of TAMs into tumoricidal phenotype. The phenotype of isolated TANs including the tumor-infiltrated endogenous and adoptive NEs was also detected. The result showed that the levels of antitumor genes including *TFN-α*, *trail*, and *lactoferrin* in TANs from the NEs@

https://doi.org/10.1021/acsnano.2c11764
ACS Nano 2023, 17, 1663−1680

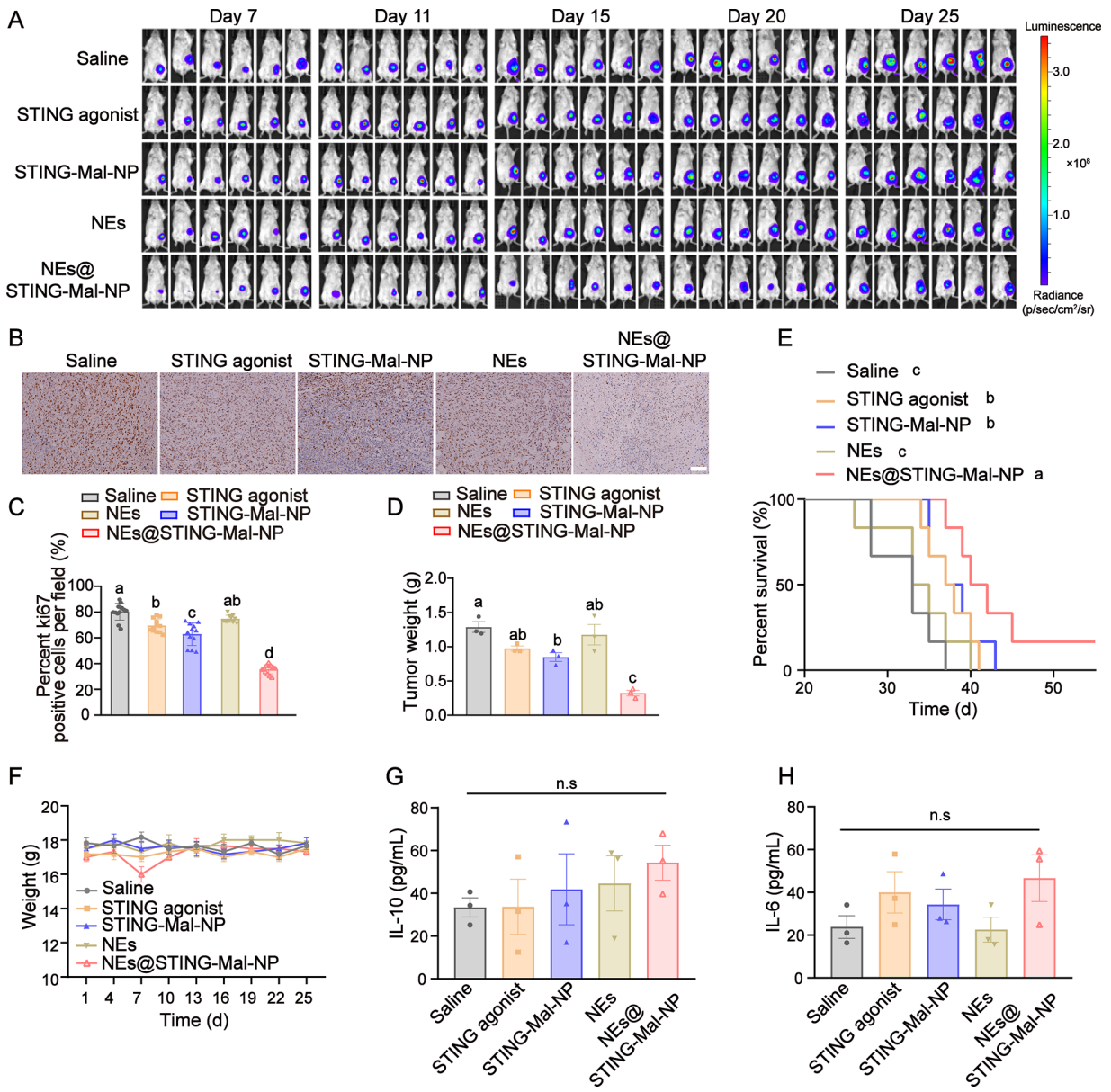

Figure 6. Antitumor efficacy of NEs@STING-Mal-NP in orthotopic 4T1-bearing mice. (A) *In vivo* bioluminescence images of mice bearing orthotopic 4T1 tumors. (B) Representative microscopic images and (C) quantifications of tumor sections immune-stained by ki67. Ki67 positive areas were quantified from each field (N = 12 fields). Scale bar, 200 μm. (D) Tumor weights of mice receiving each treatment (n = 3 mice/group). (E) Survival curves of mice receiving each treatment (n = 6 mice/group). (F) Body weights of all mice. (G, H) Measurement of serum IL-10 (G) and IL-6 (H) by ELISA (n = 3 mice/group). Data presented as means ± error bars denote SEM. Data were analyzed by one-way ANOVA with Turkey's correction (C, D, G, and H) and a long-rank (Mantel-Cox) test (E). n.s denotes no significant difference. Statistically significant differences were indicated by "abcd", and there are no significant differences between groups marked with the same letter.

STING-Mal-NP group were efficiently upregulated compared to the saline and NEs groups, while the expression of pro-tumor gene such as *CCL2* was decreased (Figure 5C). Moreover, the isolated TANs from NEs@STING-Mal-NP-treated mice produced higher levels of H_2O_2 (Figure 5D) and possessed stronger cytotoxicity against 4T1 tumor cells of more than 40% within 24 h (Figure 5E). These data sufficiently confirmed the similar phenotype transformation of TANs to tumoricidal phenotypes as TAMs due to the treatment of NEs@STING-Mal-NP. For tumor-infiltrating dendritic cells, the expressions of CD86 were upregulated (Figure 5F,G), as well as the MHC II expression (Figure 5H,I), suggesting the promoted maturation of tumor-infiltrating dendritic cells induced by NEs@STING-Mal-NP. It was well-known that dendritic cells as the typical antigen-presenting cells held the capability of activation of T cells. Thus, the capacity of tumor-infiltrating $CD8^+$T cells to secrete inflammatory cytokines, including IFNγ, TNFα, and lytic enzyme granzyme B (GzmB), was explored to evaluate the activation of T cells. We found that mice receiving the STING agonist and STING-Mal-NP showed an improved percentage of IFNγ^+, TNFα^+, and $GzmB^+$ tumor-infiltrating $CD8^+$T cells, presumably due to the moderate effect of STING agonist. In contrast, NEs@STING-Mal-NP group displayed the largest proportion of cytokine and cytolytic granule positive $CD8^+$T cells (Figure 5J,K), owing to the excellent tumor penetration of

https://doi.org/10.1021/acsnano.2c11764
ACS Nano 2023, 17, 1663−1680

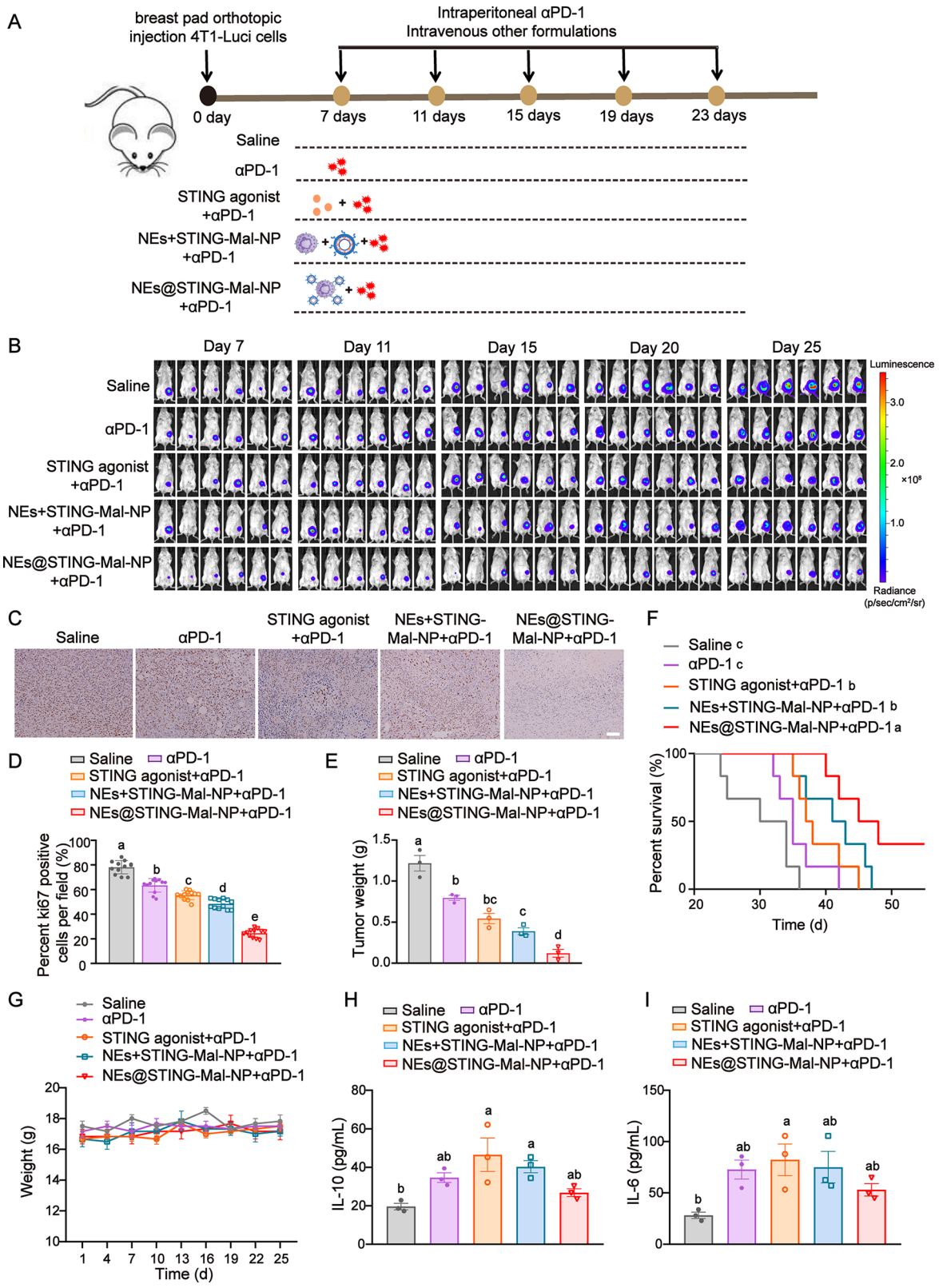

Figure 7. NEs@STING-Mal-NP sensitizing tumor to αPD-1 therapy in orthotopic 4T1 breast cancer-bearing mice. (A) Schematic illustration of the experimental design. (B) *In vivo* bioluminescence images of mice bearing orthotopic 4T1 breast cancer. (C) Representative microscopic images and (D) quantifications of tumors sections immuno-stained by ki67. Ki67 positive areas were quantified from each field (N = 12 fields). Scale bar, 200 μm. (E) Tumor weights of mice receiving each treatment (n = 3 mice/group). (F) Survival curves of mice receiving each treatment (n = 6 mice/group). (G) Body weights of all mice. (H, I) Measurement of serum IL-10 (H) and IL-6 (I) by ELISA (n = 3 mice/group). Data presented as means ± error bars denote SEM. Data were analyzed by one-way ANOVA with Turkey's correction (D, E, H, and I) and a long-rank (Mantel-Cox) test (F). Statistically significant differences were indicated by "abcd", and there are no significant differences between groups marked with the same letter.

https://doi.org/10.1021/acsnano.2c11764
ACS Nano 2023, 17, 1663−1680

STING agonist endowed by NEs and the improved entry of STING agonist into various cells. The gating strategies of Figure 5A,F,J are presented in Figure S15A,B,D, respectively.

Additionally, we evaluated the immune-memory effect of NEs@STING-Mal-NP via detection the ratio of central memory-like subset ($CD44^+CD62L^+$) of $CD8^+$T cells in tumor, blood, and spleen.[46] As shown in Figure S16, we found that the ratio of $CD44^+CD62L^+CD8^+$ T cells in tumor, blood, and spleen of mice receiving NEs@STING-Mal-NP were the highest among all the groups, indicating the effective immune-memory induced by tumor-penetrating NE cytopharmaceuticals. It can be ascribed to the enhanced accumulation of STING agonist at tumor site by NEs@STING-Mal-NP, thus activating the STING pathway and subsequent the increase of immune-memory-like subset of $CD8^+$T cells. The gating strategy of Figure S16 is presented in Figure S15E.

In short, we have demonstrated that the tumor-penetrating NE cytopharmaceuticals successfully reinvigorated the immunosuppressive tumor microenvironment into an immunogenic, tumoricidal microenvironment by effectively activating the STING pathway, not only improving the infiltration of immune cells but also remodulating their phenotypes, maturation, and activation, which suggests a potential efficacy against TNBC.

The Antitumor Effect of NEs@STING-Mal-NP. We next explored the antitumor efficacy of NEs@STING-Mal-NP *in vivo*. Mice bearing orthotopic TNBC were randomly divided into five groups and given five intravenous injections on day 7, 11, 15, 19, and 23 post-tumor inoculation with one of the following formulations: (1) saline, (2) STING agonist, (3) STING-Mal-NP, (4) NEs, and (5) NEs@STING-Mal-NP. As presented in Figure 6A, NEs@STING-Mal-NP exhibited a relatively stronger effect on the inhibition of the tumor growth, compared with other groups over 25 days. Tumors were harvested on day 25 and analyzed by immunohistochemistry to detect the expressions of ki67, a proliferation marker. As shown in Figure 6B,C, fewer ki67 positive tumor cells were observed in the NEs@STING-Mal-NP-treated group than other groups. Besides, tumors of the NEs@STING-Mal-NP group presented the smallest weight among all the groups, with a tumor inhibition rate of 70.0% (Figure 6D). Consistent with the tumor growth, 50% of TNBC-bearing mice receiving NEs@STING-Mal-NP survived for at least 40 days, compared to 33 days for saline-treated mice (Figure 6E). However, free STING agonist and STING-Mal-NP exhibited only a moderate antitumor effect, suggesting that NEs played an essential role in delivery of STING agonist throughout the tumor site and thus improving the antitumor effect.

For the safety evaluation, no noticeable reduction in body weight of all mice was found during the treatment of different formulations (Figure 6F). Meanwhile, the main organs including the heart, liver, spleen, lung, and kidney were harvested and weighed on day 25. The mice treated with NEs@STING-Mal-NP did not show any significant variations in the mass ratio of the organ to the body (Figure S17A). Besides, NEs@STING-Mal-NP showed no harm to the functions of the liver, kidney, or heart [alanine transaminase (ALT) and aspartate transaminase (AST) for liver toxicity, blood urea nitrogen (BUN), creatinine (CRE) and lactate dehydrogenase (LDH) for kidney toxicity, α-hydroxybutyrate dehydrogenase (HBDH) for heart toxicity; Figure S17B−G]. Furthermore, the histological analysis of the liver, spleen, and kidney using the HE staining evidenced that the treatment with NEs@STING-Mal-NP displayed no pathological change compared to that with saline (Figure S18). It should be noted that interleukin-6 (IL-6) and interleukin-10 (IL-10), the cytokines implicated as a central mediator of toxicity in cytokine release syndrome (CRS), were poorly released in the blood of 4T1 tumor-bearing mice after treatment with NEs@STING-Mal-NP, both at the earlier time point (4, 6, and 12 h after one injection, Figure S19) and longer time point (48 h after the last injection, Figure 6G,H), indicating that NEs@STING-Mal-NP were safe and with no risk of CRS.

Enhanced Immune Therapeutic Efficacy of Antiprogrammed Death 1 Antibody (αPD-1) via NEs@STING-Mal-NP. Having demonstrated the reactivation of the tumor microenvironment via NEs@STING-Mal-NP, we finally evaluated whether it could sensitize tumor to ICIs such as antiprogrammed death-1 antibody (αPD-1) in TNBC therapy. The orthotopic breast cancer (4T1-Luci)-bearing mice are known to express programmed cell death-ligand 1 (PD-L1)[47] but are largely resistant to the PD-L1/PD-1 blockade owing to the highly immunosuppressive microenvironment.[48] To improve the effectiveness of αPD-1, 4T1-Luci bearing mice were intravenously injected with NEs@STING-Mal-NP or other formulations for 5 injections starting on day 7 after inoculation, each combining with intraperitoneal administration of αPD-1 (Figure 7A).

During the treatment, αPD-1 monotherapy showed the minimal therapeutic effect, while combined with NEs@STING-Mal-NP it displayed the strongest inhibition on tumor growth (Figure 7B), which was further evidenced by the ki67 immunohistochemistry (Figure 7C, D) and the tumor weight with an inhibition ratio of about 90.6% (Figure 7E). Notably, 33% of TNBC-bearing mice (2/6) that received NEs@STING-Mal-NP in combination with αPD-1 exhibited complete response, with no tumor burden for survival at least 55 d after the therapy cessation (Figure 7F). In short, intravenously administration of NEs@STING-Mal-NP synergized with αPD-1 could produce complete and durable responses, offering a therapy regimen of combining STING agonists and αPD-1 for treatment of poorly immunogenic cancer, such as TNBC.

To further support the potential for clinical application of NEs@STING-Mal-NP combined with αPD-1, we investigated the safety of NEs@STING-Mal-NP including the body weight, organ index (organ weight/body weight), pathological analysis, blood biochemistry, and blood routine, especially the inflammatory factors storm, which could be triggered by αPD-1 *in vivo*. The results showed that both NEs@STING-Mal-NP- and αPD-1-treated mice showed no detectable significant changes in body weights (Figure 7G) and organ indexes (Figure S20A), compared to saline-treated mice. Moreover, blood biochemistry and complete blood count also showed no significant changes (Figure S20B−G and S21). The pathological analysis results also displayed no obvious tissue damage in all experiment groups (Figure S22). Importantly, IL-10 and IL-6 from NEs@STING-Mal-NP and αPD-1 combined groups exhibited fewer expressions than that from αPD-1 monotherapy or combined with STING agonist groups, respectively (Figure 7H,I), which could be ascribed to the highly tumor-penetrating efficiency of NEs@STING-Mal-NP in the tumor site, thus reducing the undesired side effects caused by STING agonist. Overall, NEs@STING-Mal-NP increased the response rates and the durability of remission of

https://doi.org/10.1021/acsnano.2c11764
ACS Nano 2023, 17, 1663−1680

αPD-1 with safety *in vivo*, possessing the potential to treat the poor immunogenic TNBC patients in the clinic.

CONCLUSIONS

We have successfully developed tumor-penetrating neotype NE cytopharmaceuticals by backpacking liposomal STING agonist on the surface of NEs. The creative cytopharmaceuticals can proactively transmigrate the tumor vascular endothelium and extravasate into the TNBC, resulting in highly improved tumor penetration of STING agonists. Moreover, the backpacked liposomal STING agonists can be stimuli-released in response to the tumor environment and improved the following uptake by tumor cells and tumor infiltrating immune cells. Thus, they can effectively reactivate the STING signaling pathway in TME, leading to the reinvigoration of immunosuppressive TME to immunogenic states, and finally achieve the potent antitumor effect against TNBC, especially sensitizing tumors to the immune checkpoint inhibitors. This study offers an orchestrated tool for boosting antitumor immunity as well as the response rates and remission durability of immune checkpoint inhibitors in TNBC immunotherapy, which possesses wide future perspectives in the treatment of immunologically "cold" tumors.

MATERIALS AND METHODS

Materials. STING agonist (DMXAA) was purchased from MedChemExpress (MCE, Shanghai, China). ELISA kit was purchased from Elabscience (Wuhan, China). TCEP·HCl, Collagenase IV, Ce6 and hyaluronidase were purchased from Sigma (America). Ionomycin (Cat No.S0401ES03) and DNAase I (Cat No. 10607ES15) were purchased from YEASEN (Shanghai, China). HiScript II Q RT SuperMix for qPCR and AceQ qPCR SYBR Green Master Mix were purchased from Vazyme Biotech Co., Ltd. (Nanjing, China). Percoll, Hoechst, brefeldin A, hydrogen peroxide assay kit, RBC Lysis Buffer, and PMA were purchased from Beyotime (Shanghai, China). All fluorescent antibodies were obtained from BioLegend (America). Fetal bovine serum (FBS), Dulbecco's modified Eagle medium (DMEM) high-glucose medium, trypsin, penicillin-streptomycin, and Hank's buffer were obtained from Thermo Fisher Scientific (America). HUVEC and 4T1 cells were purchased from the American Type Culture Collection (ATCC, America). The female BALB/c mice (18−22 g) were purchased from Qinglongshan Animal Breeding Ground (Nanjing, China) and kept under standard housing conditions. All the animal experiments were performed in compliance with the Guide for Care and Use of Laboratory Animals, approved by China Pharmaceutical University.

Preparation and Characterization of STING-Mal-NP. SPC (70 mg), cholesterol (12 mg), SA_2 (10 mg), BA (2.2 mg), and STING agonist (DMXAA, 7 mg) were dissolved in 5 mL of the mixture of $CHCl_3$ and MeOH (3:2, v: (v). After removing the organic solvents by rotary evaporation at 40 °C, a thin lipid film was formed and further dried under vacuum overnight to remove the remaining organic solvents. Then, the lipid film was hydrated in 5 mL of distilled water at 37 °C for 30 min. The STING agonist loaded cationic liposome (STING-Lip) was obtained after the sonication (15 min, 4 °C) and the filtration through a 0.22 μm microfiltration membrane. Finally, 5 mL of STING-Lip (18.4 mg/mL) was gently mixed with 3.787 mL of HA-Mal (10 mg/mL) to obtain the STING-Mal-NP after incubation for 20 min at room temperature.

Similarly, fluorescent liposomes were obtained by the same method as for STING-Lip except for the addition of DHPE-Rhodamine B (25 μL, 5 mg/mL) in the mixture of $CHCl_3$ and MeOH (3:2, v: (v). Then fluorescent liposomes were gently mixed with HA or HA-Mal to obtain the STING-NP-RhoB or STING-Mal-NP-RhoB after the incubation for 20 min at room temperature.

STING-Mal-NP were diluted in 10 mM PBS, and the particle size and zeta potential were measured using a Brookhaven Zetaplus. For transmission electron microscopy (TEM) image, STING-Mal-NP were dropped onto a copper grid (300 mesh) and stained by phosphotungstic acid (0.5%) for 5 min, followed by imaging by Transmission Electron Microscope (120 kV Hitachi HT-7700).

For assessment of the entrapment efficiency of DMXAA in STING-Mal-NP, 20 μL of STING-Mal-NP was mixed with 980 μL of methanol with a vortex for 5 min and centrifuged at 10000*g* for 10 min. The supernatant (20 μL) was then collected and the concentration of STING agonist was determined by High Performance Liquid Chromatography (HPLC, Shimadzu LC-2010A). The entrapment efficiency (EE)% = $m_{\text{STING agonist detected}}/m_{\text{STING agonist fed}} \times 100\%$, $m_{\text{STING agonist}}$ was calculated by the concentration of STING agonist multiplied by the total volume, while $m_{\text{STING agonist fed}}$ was the weight of feeding DMXAA. For drug loading percentage of DMXAA, STING-Mal-NP was lyophilized first. Then, 10 mg of lyophilized STING-Mal-NP was dissolved in 1 mL of PBS (10 mM), which was detected by HPLC following the procedure before. The drug loading (DL)% = $m_{\text{STING agonist}}/m_{\text{STING-Mal-NP}} \times 100\%$, $m_{\text{STING agonist}}$ was calculated by the concentration of STING agonist multiplied by the total volume, while $m_{\text{STING-Mal-NP}}$ was the weight of lyophilized STING-Mal-NP of 10 mg.

To evaluate the stability *in vitro*, STING-Mal-NP was respectively incubated with RPMI 1640 complete medium, 20 mM acetate buffer (pH 6.5), and 20 mM HEPES buffer (pH 7.4) at a volume ratio of 1:1 and then placed in a 37 °C water bath. The particle size of STING-Mal-NP at different time points (0, 2, 4, 6, 8, 10, and 24 h) was detected using Brookhaven Zetaplus.

For HA degradation, STING-Mal-NP was respectively mixed with 20 mM HEPES buffer (pH 7.4, 120 ng/mL HAase) or 20 mM acetate buffer (pH 6.5, 1 mg/mL HAase) at a volume ratio of 1:1 and then placed at 37 °C. At different time points (0.5, 1, 2, 3, 4, and 5 h), the supernatant was harvested after centrifugation (1000 g, 3 min). The degradation amounts of HA-Mal in supernatants was quantified as previously reported. Briefly, 50 μL different concentrations of HA-Mal standard solutions (0.1−2 mg/mL) or supernatants were added to a 96-well plate. After adding 50 μL of 0.2 M sodium acetate buffer for 10 min at 37 °C, 100 μL of 10 mM hexadecyltrimethylammonium bromide (CTAB) solution was added and the absorbance was read within 10 min at 570 nm by microplate reader. The degradation amount of HA-Mal was calculated by subtracting the amount in the supernatant fraction from the initial amount added to the reaction mixture.

Preparation and Characterization of NEs@STING-Mal-NP. Bone marrow was flushed from femur and tibia bones of ICR mice with RMPI 1640 including 1% penicillin-streptomycin. After centrifugation at 200 g for 3 min and lysis by red blood cell lysis buffer for 3 min, the unicellular suspension was added into a Percoll mixture solution consisting of 55%, 65% and 75% of Percoll in PBS and further centrifugated at 500 g for 30 min. Finally, the NEs were recovered at the interface of 65% and 75% and washed with ice-cold PBS twice.

Fresh NEs (1×10^6 cells/mL) were pipetted into a sterile tube and cultured with 0.5 mM TCEP for 10 min at 4 °C. Then, the NEs were further incubated with STING-Mal-NP at a STING agonist concentration of 80 μg/mL for 60 min at 37 °C. After washing with ice-cold PBS thrice, NEs@STING-Mal-NP was obtained. The concentration of STING agonist in NEs@STING-Mal-NP was determined by HPLC.

For the preparation of NEs conjugated with fluorescent nanoparticles, NEs (1×10^6 cells/mL) were incubated with 0.5 mM TCEP or 1640 medium for 10 min at 4 °C. After washing with PBS, STING-Mal-NP-RhoB or STING-NP-RhoB was incubated with cells for 60 min at 37 °C. After washing with PBS, the NEs conjugated with fluorescent nanoparticles were stained with Hoechst 33342, fixed with 4% paraformaldehyde (PFA), and used for confocal imaging and flow cytometry analysis.

To calculate the number of nanoparticles backpacked on the surface of NEs, NEs (1×10^6 cells) were first incubated with 0.5 mM TCEP at 4 °C for 10 min, and then the cells were incubated with the STING-Mal-NP or STING-NP solution in 1 mL for 60 min. The

https://doi.org/10.1021/acsnano.2c11764
ACS Nano 2023, 17, 1663−1680

concentration of STING-Mal-NP or STING-NP in the solution was measured with Nanoparticle Tracking Analyzer (Zetaview QUATT, Particle Metrix). The nanoparticle number backpacked on the surface of per NEs was calculated as follows: $(n_{\text{before STING-Mal-NP}} - n_{\text{after STING-Mal-NP}})/10^6$ or $(n_{\text{before STING-NP}} - n_{\text{after STING-NP}})/10^6$, where $n_{\text{before STING-Mal-NP}}$ and $n_{\text{before STING-NP}}$ were the counted numbers of nanoparticles in the solution before the incubation of STING-Mal-NP or STING-NP with NEs, while $n_{\text{after STING-Mal-NP}}$ and $n_{\text{after STING-NP}}$ were the counted numbers of nanoparticles in the supernatant after the incubation of STING-Mal-NP or STING-NP with NEs.

The stability of STING agonist backpacked on the surface of NEs was evaluated under the normal physiological condition. Briefly, NEs@STING-Mal-NP (1×10^6 cells/well) were seeded in sterile tubes and then incubated with RPMI 1640 medium for different periods (0, 1, 3, 5, and 7 h). The amounts of STING agonist in the NEs@STING-Mal-NP were determined using HPLC.

The release profiles of STING agonist from NEs@STING-Mal-NP were evaluated under the mimetic tumor condition (pH 6.5, 0.5 mg/mL HAase). NEs@STING-Mal-NP (1×10^6 cells/well) were seeded in sterile tubes and then incubated with RPMI 1640 medium (pH 6.5) containing 0.5 mg/mL of HAase for different periods (0, 1, 2, 3, 5, 7, and 9 h). The amounts of STING agonist in the NEs@STING-Mal-NP and the supernatant medium were respectively determined using HPLC.

Evaluation of Cell Viability and Membrane Protein of NEs@STING-Mal-NP. For viability analysis, 1×10^6 NEs and NEs@STING-Mal-NP were cultured in RPMI 1640 medium. At 0, 1, 2, 4, 6, or 8 h, the cells were collected for the viability assay using the Annexin V-FITC/PI Apoptosis Detection Kit (Vazyme Biotech Co., Ltd.) and trypan blue staining.

NEs@STING-Mal-NP and unconjugated NEs were collected and disrupted using 300 μL of 1% SDS lysis buffer supplemented with benzonase and protease inhibitor cocktail, and the cell debris was removed by centrifugation at 16000*g* for 30 min. Cellular proteins were quantified using a bicinchoninic acid (BCA) assay kit (Beyotime Biotechnology) according to the instruction of the manufacturer. The proteins were diluted to 0.75 μg/μL with a total volume of 281 μL, reduced by 2 mM DTT for 30 min at 37 °C, and alkylated by 20 mM IDDA for 30 min at 37 °C in the dark under rotator stirring. Each sample was divided equally into two tubes and precipitated with 600 μL of methanol or 150 μL of chloroform and 450 μL of ddH_2O. The precipitate was washed twice with 1 mL of methanol by centrifugation at 13000*g* for 15 min. 100 μL of 8 M urea was added to each tube to dissolve the proteins, and the two tubes of identical samples were combined. For proteomics analysis, the proteins were digested with a protease:protein ratio of 1:200 at room temperature for 3−4 h. 10% TFA of 1/10 sample volume was added to adjust the pH to ≤3. The samples were then desalted by HLB-c18-1 cm^3 column, eluted by 1 mL of 50% ACN and 0.1% FA, and lyophilized. The lyophilized samples were resuspended with 150 μL of pH 8.03 200 mM HEPES solution under vortex and fractionated into 12 fractions by a BP-HRP-HPLC system. Each elution fraction was injected into an Orbitrap Fusion Lumos (Thermo) for mass spectrometry. Gene Ontology (GO) enrichment analysis of expressed proteins was performed using the Cytoscape plugin BiNGO (3.0.4). Proteins related to the biological processes of neutrophil viability, chemotaxis, extravasation, and immune effectors were sorted out and shown on a volcano plot.

Quantitative PCR with Reverse Transcription (RT-qPCR). Cells (4T1 tumor cells, macrophages, or dendritic cells) were respectively incubated with RPMI 1640 medium, STING agonist (10 μg/mL), STING-Mal-NP (10 μg/mL for STING agonist, HAase), NEs (3.1×10^6 cells), or NEs@STING-Mal-NP (3.1×10^6 cells, 10 μg/mL for STING agonist, HAase) for 12 h. Then the cells were collected, centrifuged at 300*g* for 3 min, and washed with PBS twice. The total RNA was extracted by the TRNzol reagent according to a standard protocol. cDNA was synthesized with HiScript II Q RT SuperMix for qPCR kit (Vazyme Biotech Co., Ltd.) and analyzed via real-time RT-PCR using the AceQ qPCR SYBR Green Master Mix kit (Vazyme Biotech Co., Ltd.) and specific primers for mouse *INF-β*, *CCL5*, *CXCL9*, *CXCL10*, *CXCL1*, *CD80*, and *CD86*. Additionally, the culture supernatant of the above groups treated with dendritic cells was collected and incubated with NEs for another 12 h. After that, the total RNA of NEs was also extracted and cDNA was synthesized for the measurement the expressions of *TNF-α*, *ICAM-1*, *TRAIL*, *Lactoferrin*, and *CCL2*.

Flow Cytometric Analysis of Marker/Effector Expressions of Macrophages and Dendritic Cells. Cells (macrophages or dendritic cells) were respectively cultured and treated as mentioned above for 12 h. Then cells were recovered, centrifuged at 300*g* for 3 min, and washed with PBS twice. Cells were diluted to a concentration of 2×10^7 cells/mL in PBS for staining with fluorescent antibodies for 30 min, washed with PBS, and analyzed by flow cytometry with APC-CD86 antibody for dendritic cells and Alexa Fluor 488-CD206 antibody for M2 macrophages.

Evaluation of Hydrogen Peroxide Secretion and Tumor Cytotoxicity of NEs. NEs were cultured and treated with the culture supernatant of above groups treated dendritic cells for 12 h. Then the cells were collected, centrifuged at 300*g* for 3 min, and washed with PBS twice. After incubation with 100 nM PMA for 15 min, the hydrogen peroxide concentration of the supernatant was determined using hydrogen peroxide assay kit (Beyotime).

In order to evaluate the tumor cytotoxicity of NEs after treatment with the culture supernatant of above groups treated dendritic cells, luciferase-transfected 4T1-cells (4T1-Luci) were plated in 96-well plates for 24 h, followed by incubation with NEs with or without treatment as mentioned above for 12 h at a ratio of target cell: effector cell of 1:10. The cell viability was evaluated using the luciferase reporter assay system.

The Expression of IFN-β by Enzyme-Linked Immunosorbent Assay (ELISA). Cells (4T1 tumor cells, macrophages, or dendritic cells) were respectively cultured and treated as mentioned above for 12 h. The supernatant was collected and centrifuged at 750*g* for 10 min. Then, the IFN-β concentration was assessed using a Mouse IFN-β ELISA Kit (Elabscience).

The Extravasation and Tumor Penetration of NEs@STING-Mal-NP. For investigation of the expressions of chemotaxis and extravasation-related receptors, NEs or NEs@STING-Mal-NP (1×10^6 cells) were respectively incubated with the APC−CCR2 antibody, FITC-CD62L antibody, Alexa Fluor 488-CD11a antibody or Alexa Fluor 647-CD11b antibody (BioLegend) for 30 min and then washed with ice-cold PBS twice. The fluorescence intensity was determined using flow cytometry.

The chemotaxis of NEs@STING-Mal-NP was investigated using a transwell migration assay (3 μm, 6.5 mm, Corning). Briefly, NEs and NEs@STING-Mal-NP (1×10^6 cells) were seeded in 500 μL of RPMI 1640 complete medium on the top of the membrane chamber, followed by submerging into wells containing 100% 4T1 TCM, 50% 4T1 TCM or RPMI 1640 media. After 8 h, the inset was removed. The cells in the wells were counted in five random × 10 brightfields of views by Olympus microscopy (FV1100). The chemotaxis index $((N_{\text{4T1 TCM}} - N_{\text{control}})/N_{\text{control}})$ was calculated, where $N_{\text{4T1 TCM}}$ and N_{control} are the counted numbers of NEs in the lower chamber after incubation with NEs or NEs@STING-Mal-NP in the presence or absence of 4T1 TCM, respectively.

To evaluate the tumor vascular extravasation ability, a transwell assay with a human umbilical vein endothelial cell (HUVEC) monolayer was applied. Transwells were coated with 50 μL of 2% gelatin overnight. Then HUVECs were seeded (1×10^5 cells/well) on the transwell membrane in DMEM complete media and cultured until the confluent HUVECs exhibited a mean TEER of 300 $\Omega \cdot cm^2$. After being stimulated with TNFα for 0.5 h, NEs or NEs@STING-Mal-NP (1×10^6 cells) were seeded in the upper chamber containing a HUVEC monolayer with 500 μL of RPMI 1640 medium, followed by submerging into wells containing 100% 4T1 TCM, 50% 4T1 TCM, or unconditioned media. After 8 h, the inset was removed. The cells in the wells were counted in five random × 10 bright fields of view by Olympus microscopy. The tumor vascular extravasation ability $((N_{\text{4T1 TCM}} - N_{\text{control}})/N_{\text{control}})$ was calculated as mentioned above.

The tumor penetration of NEs@STING-Mal-NP was evaluated as follows. 3×10^6 4T1 cells were injected into the fourth left mammary

https://doi.org/10.1021/acsnano.2c11764
ACS Nano 2023, 17, 1663−1680

fat pad of 6−8 weeks BALB/c mouse in 100 μL of PBS. The tumor size was measured every other day via a vernier caliper, and the tumor volume was calculated using the equation $V = L \times W \times W/2$. When tumor volume reached about 100 mm^3, the mice were intravenously injected with Ce6, Ce6-Mal-NP, and NEs@Ce6-Mal-NP at the same dose. At different times postinjection, the images were acquired by Maestro *in vivo* imaging system (Cambridge Research & Instrumentation, USA). The fluorescence of Ce6 in liver and tumor were quantified. At 48 h postinjection, the mice were sacrificed. Tumor and other tissues were harvested for *ex vivo* imaging through MaestroTM *ex vivo* imaging system.

To further demonstrate the *in vivo* tumor penetration and biodistribution of NEs@STING-Mal-NP, NEs and NEs@STING-Mal-NP were labeled with DIR for convenient imaging. Then 4T1 tumor-bearing mice were intravenously injected with DIR, NEs-DIR, and NEs-DIR@STING-Mal-NP, respectively. At 4, 6, 12, 24, and 48 h postinjection, mice were sacrificed after the blood collection, and the tissues including tumor, heart, liver, spleen, lung, and kidney were harvested for *ex vivo* imaging systems (Cambridge Research & Instrumentation, USA). The collected tumors were then digested by collagenase IV for 45 min at 37 °C and treated with red blood cell lysis buffer to obtain a single-cell suspension at a final concentration of 2×10^7 cells/mL in PBS. Then, the DIR labeled NEs in tumor were analyzed by flow cytometry. Moreover, tumors and tissues were weighed and homogenized in saline. For analysis of STING agonist quantity, the homogenate was diluted with 10% $NaHCO_3$ aqueous solution and mixed with acetonitrile, followed by vortex for 5 min and centrifugation at 12000 rpm for 10 min. Then, 200 μL of supernatant was quantified by HPLC to determine the concentration of STING agonist in tumor and tissues. The blood collected at 4, 6, and 12 h was centrifugated at 12000 rpm for 10 min to collect the serum and then analyzed for IL-6 and IL-10 concentration via ELISA Kit (Elabscience).

The Phenotypes and STING-Related Gene Expressions of Tumor-Infiltrating Immune Cells in 4T1-Luci Orthotopic Breast Cancer Model. 3×10^6 4T1-Luci cells were injected into the fourth left mammary fat pad of 6−8 weeks BALB/c mouse in 100 μL of PBS on day 0. The tumor-bearing mice were randomly divided into five groups and received saline, STING agonist (3 mg/kg), STING-Mal-NP (3 mg/kg for STING agonist), NEs (2×10^7), and NEs@STING-Mal-NP (2×10^7, 3 mg/kg for STING agonist) by intravenous injection on day 7, 11, 15, 19, and 23 after tumor inoculation. Then, the 4T1-Luci orthotopic breast cancer-bearing mice were sacrificed and the tumors were collected at day 25.

For evaluation of the STING-related gene expressions and IFN-β concentration of 4T1 tumor tissues, the total mRNA in 50 mg of tumors was extracted by the TRIZOL Reagent (Life Technologies) according to the protocol of the manufacturer. cDNA synthesis and qPCR quantifications of *INF-β*, *CCL5*, *CXCL9*, *CXCL10*, and *CXCL1* transcription were performed as described above. Additionally, the amount of IFN-β in the 4T1 tumors was detected using an ELISA kit (Elabscience).

For flow cytometry analysis of the phenotypes of tumor-infiltrating immune cells, the tumors were digested by the collagenase IV for 45 min at 37 °C and treated with the red blood cell lysis buffer to obtain a single-cell suspension, which was then diluted to a concentration of 2×10^7 cells/mL in PBS. Then, the cells were stained with separate fluorescent-labeled antibody for 30 min, washed with PBS twice, and analyzed by flow cytometry. For TAMs, the cells were stained with PE-CD45 antibody, APC-F4/80 antibody, and AF488-CD206 antibody. For tumor-infiltrating dendritic cells, the cells were stained with PE-CD45 antibody, AF647-CD11c antibody, AF488-CD86 antibody, and APC-MHC II antibody. For tumor-infiltrating $CD8^+$T cells, the cells were gradient centrifugated by 40 to 70% Percoll and then stimulated with ionomycin and PMA for 4 h in the presence of brefeldin A, followed by staining with BV421-CD45 antibody, APC-CD3 antibody, APC-Cy7-CD8 antibody, AF488-GzmB antibody, PE-IFNγ antibody, and PE-Cy5.5-TNFα antibody. All data were analyzed using FlowJo software.

For STING-related gene expressions and antitumor capacity of TANs, the single-cell suspension was gradient centrifugated by 55, 65 to 75% Percoll to obtain tumor-infiltrated NEs. The gene expressions of TANs including *TNF-α*, *ICAM-1*, *TRAIL*, *Lactoferrin*, and *CCL2* were measured by using RT-qPCR. The H_2O_2 release and the cytotoxicity of TANs against 4T1-Luci cells were analyzed as mentioned above.

Antitumor Efficacy of NEs@STING-Mal-NP in 4T1-Luci Orthotopic Breast Cancer Model. The 4T1-Luci tumor-bearing mice were randomly divided into five groups and received saline, STING agonist (3 mg/kg), STING-Mal-NP (3 mg/kg for STING agonist), NEs (2×10^7), and NEs@STING-Mal-NP (2×10^7, 3 mg/kg for STING agonist) by intravenous injection on day 7, 11, 15, 19, and 23 after tumor inoculation. The tumor growths were monitored and imaged for bioluminescence on day 7, 11, 15, 20, and 25, respectively. The animal survival was recorded every day and the body weight of all mice were monitored every 2 days. On day 25, mice were sacrificed and the tumors were harvested and weighed. Heart, liver, spleen, lung, and kidney of the mice were collected and weighed to calculate the organ index. Additionally, the tumors and organs were dissected, embedded in paraffin, sectioned, and stained with rabbit antimouse ki67 and hematoxylin and eosin (H&E) using routine methods. The sections were photographed using Microscope BX53 (Olympus) and analyzed by ImageJ (Fiji, 1.51n) with the ImmunoRatio 1.0c plugin. The serum samples from each group of mice were collected on day 25 after tumor inoculation, and the quantities of ALT, AST, CRE, BUN, LDH, and HBDH were respectively determined per kit instructions, and IL-6 and IL-10 concentrations were analyzed via ELISA kit (Elabscience).

NEs@STING-Mal-NP Combined with PD-1 Antibody (αPD-1) for Treating 4T1-Luci Orthotopic Breast Cancer. The 4T1-Luci tumor-bearing mice were randomly divided into five groups and received saline, αPD-1 (7.5 mg/kg, i.p), STING agonist (3 mg/kg, i.v) + αPD-1 (7.5 mg/kg, i.p), NEs (2×10^7, i.v) + STING-Mal-NP (3 mg/kg for STING agonist, i.v) + αPD-1 (7.5 mg/kg, i.p), and NEs@STING-Mal-NP (2×10^7, 3 mg/kg for STING agonist, i.v) + αPD-1 (7.5 mg/kg, i.p) on day 7, 11, 15, 19, and 23 after tumor inoculation. The tumor growth was monitored and imaged for bioluminescence on day 7, 11, 15, 20, and 25, respectively. The animal survival was recorded every day and the body weight of all mice were monitored every 2 days. On day 25, mice were sacrificed and the tumors were harvested and weighed. Heart, liver, spleen, lung, and kidney of the mice were also collected and weighed to calculate the organ index. Additionally, the tumors and organs were dissected, embedded in paraffin, sectioned, and stained with rabbit antimouse ki67 and hematoxylin and eosin (H&E) using routine methods. The sections were photographed using Microscope BX53 (Olympus) and analyzed by ImageJ (Fiji, 1.51n) with the ImmunoRatio 1.0c plugin. The serum samples from each group of mice were collected on day 25 after tumor inoculation, the quantities of ALT, AST, CRE, BUN, LDH, and HBDH were respectively determined per kit instructions, and IL-6 and IL-10 concentrations were analyzed via ELISA kit (Elabscience).

Statistical Analysis. Statistical analyses were performed using GraphPad Prism 8.0. All plots show mean ± SEM. One-way ANOVA test and two-way ANOVA with Tukey's correction were used for comparisons of multiple groups and a Student's unpaired *t*-test was used for two-group comparisons in the appropriate conditions. A log-rank (Mantel-Cox) test was used to analyze survival differences. Statistical significance was set at $^*P < 0.05$, $^{**}P < 0.01$, $^{***}P < 0.001$, and $^{****}P < 0.0001$, n.s: no significant difference, or indicated by "abcd" that there are no significant differences between groups marked with the same letter.

ASSOCIATED CONTENT

Supporting Information

The Supporting Information is available free of charge at https://pubs.acs.org/doi/10.1021/acsnano.2c11764.

https://doi.org/10.1021/acsnano.2c11764
ACS Nano 2023, 17, 1663−1680

Materials and methods including the detailed methods of cell culture, isolated and polarized the primary cells, the preparations of the fluorescent nanoparticles and 4T1 TCM, Western blot, and immune memory experiments, as well as Figures S1−S22. Figure S1, particle size and zeta potential of STING-Mal-NP; Figure S2, optimization of reduction condition and click reaction; Figures S3 and S4, cell viability and TMT-based quantitative proteomics of NEs@STING-Mal-NP; Figure S5, Western blot assay of phospho-STING (Ser365) in 4T1 cells, BMDM, and BMDC after different treatment; Figure S6, IFN-β secretion of immune cells; Figure S7, Western blot analysis of phospho-STING (Ser365) in NEs and NEs@STING-Mal-NP; Figure S8, qPCR analysis of STING-related gene expression in NEs@STING-Mal-NP; Figures S9−S11, biodistribution of NEs and STING agonist *in vivo*; Figures S12−S14, expressions of STING related genes and secreted INF-β proteins and immune cells infiltrated in tumors from mice receiving different treatments; Figure S15, gating strategy of flow cytometry analysis; Figure S16, immune-memory phenotype of $CD8^+$T cells in 4T1 orthotopic tumors after the treatment with NEs@STING-Mal-NP; Figures S17−S22, safety evaluation in 4T1 orthotopic breast tumor-bearing mice (PDF)

AUTHOR INFORMATION

Corresponding Authors

Can Zhang − *State Key Laboratory of Natural Medicines, Jiangsu Key Laboratory of Drug Discovery for Metabolic Diseases, Center of Advanced Pharmaceuticals and Biomaterials, China Pharmaceutical University, Nanjing 210009, P.R. China*; orcid.org/0000-0003-3529-5438; Email: zhangcan@cpu.edu.cn

Caoyun Ju − *State Key Laboratory of Natural Medicines, Jiangsu Key Laboratory of Drug Discovery for Metabolic Diseases, Center of Advanced Pharmaceuticals and Biomaterials, China Pharmaceutical University, Nanjing 210009, P.R. China*; Email: jucaoyun@cpu.edu.cn

Authors

Meixi Hao − *State Key Laboratory of Natural Medicines, Jiangsu Key Laboratory of Drug Discovery for Metabolic Diseases, Center of Advanced Pharmaceuticals and Biomaterials, China Pharmaceutical University, Nanjing 210009, P.R. China*

Lulu Zhu − *State Key Laboratory of Natural Medicines, Jiangsu Key Laboratory of Drug Discovery for Metabolic Diseases, Center of Advanced Pharmaceuticals and Biomaterials, China Pharmaceutical University, Nanjing 210009, P.R. China*

Siyuan Hou − *State Key Laboratory of Natural Medicines, Jiangsu Key Laboratory of Drug Discovery for Metabolic Diseases, Center of Advanced Pharmaceuticals and Biomaterials, China Pharmaceutical University, Nanjing 210009, P.R. China*

Sijia Chen − *State Key Laboratory of Natural Medicines, Jiangsu Key Laboratory of Drug Discovery for Metabolic Diseases, Center of Advanced Pharmaceuticals and Biomaterials, China Pharmaceutical University, Nanjing 210009, P.R. China*

Xiuqi Li − *State Key Laboratory of Natural Medicines, Jiangsu Key Laboratory of Drug Discovery for Metabolic Diseases, Center of Advanced Pharmaceuticals and Biomaterials, China Pharmaceutical University, Nanjing 210009, P.R. China*

Kaiming Li − *State Key Laboratory of Natural Medicines, Jiangsu Key Laboratory of Drug Discovery for Metabolic Diseases, Center of Advanced Pharmaceuticals and Biomaterials, China Pharmaceutical University, Nanjing 210009, P.R. China*

Nianci Zhu − *State Key Laboratory of Natural Medicines, Jiangsu Key Laboratory of Drug Discovery for Metabolic Diseases, Center of Advanced Pharmaceuticals and Biomaterials, China Pharmaceutical University, Nanjing 210009, P.R. China*

Shanshan Chen − *State Key Laboratory of Natural Medicines, Jiangsu Key Laboratory of Drug Discovery for Metabolic Diseases, Center of Advanced Pharmaceuticals and Biomaterials, China Pharmaceutical University, Nanjing 210009, P.R. China*

Lingjing Xue − *State Key Laboratory of Natural Medicines, Jiangsu Key Laboratory of Drug Discovery for Metabolic Diseases, Center of Advanced Pharmaceuticals and Biomaterials, China Pharmaceutical University, Nanjing 210009, P.R. China*

Complete contact information is available at: https://pubs.acs.org/10.1021/acsnano.2c11764

Author Contributions

‡Meixi Hao and Lulu Zhu contributed equally. Meixi Hao designed and conducted all experiments, analyzed the data, and wrote the original manuscript. Lulu Zhu conducted all experiments, analyzed the data, and wrote the original manuscript. Siyuan Hou conceived the research ideas and designed mice experiments. Sijia Chen and Xiuqi Li assisted in analyzing the data and wrote the manuscript. Lingjing Xue assisted in analyzing the data. Nianci Zhu and Shanshan Chen assisted in mice experiments. Caoyun Ju supervised all animal experiments and wrote the manuscript. Can Zhang conceived the project and supervised all the experiments.

Notes

The authors declare no competing financial interest.

ACKNOWLEDGMENTS

This work was supported by the National Natural Science Foundation of China (81930099, 82130102, 81773664, 92159304, 82073785, 82104102), the Natural Science Foundation of Jiangsu Province (BK20212011, BK20190558), "Double First-Class" University project (CPU2022QZ05), Technology innovation project of Nucleic acid drug from National Center of Technology Innovation for Biopharmaceuticals (NCTIB2022HS01014), 111 Project from the Ministry of Education of China and the State Administration of Foreign Expert Affairs of China (No. 111-2-07, B17047), and the Project Program of State Key Laboratory of Natural Medicines (China Pharmaceutical University, No. SKLNMZZ202223).

REFERENCES

(1) Garrido-Castro, A. C.; Lin, N. U.; Polyak, K. Insights into Molecular Classifications of Triple-Negative Breast Cancer: Improv-

ing Patient Selection for Treatment. *Cancer Discov* **2019**, *9* (2), 176−198.
(2) Andre, F.; Zielinski, C. C. Optimal strategies for the treatment of metastatic triple-negative breast cancer with currently approved agents. *Ann. Oncol* **2012**, *23*, vi46−51.
(3) Jiang, Y. Z.; Liu, Y.; Xiao, Y.; Hu, X.; Jiang, L.; Zuo, J.; Ma, D.; Ding, J.; Zhu, X.; Zou, J.; Verschraegen, C.; Stover, D. G.; Kaklamani, V.; wang, Z. H.; Shao, Z. M. Molecular subtyping and genomic profiling expand precision medicine in refractory metastatic triple-negative breast cancer: the FUTURE trial. *Cell Res.* **2021**, *31* (2), 178−186.
(4) Bianchini, G.; De Angelis, C.; Licata, L.; Gianni, L. Treatment landscape of triple-negative breast cancer - expanded options, evolving needs. *Nat. Rev. Clin Oncol* **2022**, *19* (2), 91−113.
(5) Gruosso, T.; Gigoux, M.; Manem, V. S. K.; Bertos, N.; Zuo, D.; Perlitch, I.; Saleh, S. M. I.; Zhao, H.; Souleimanova, M.; Johnson, R. M.; Monette, A.; Ramos, V. M.; Hallett, M. T.; Stagg, J.; Lapointe, R.; Omeroglu, A.; Meterissian, S.; Buisseret, L.; Van den Eynden, G.; Salgado, R.; Guiot, M. C.; Haibe-Kains, B.; Park, M. Spatially distinct tumor immune microenvironments stratify triple-negative breast cancers. *J. Clin Invest* **2019**, *129* (4), 1785−1800.
(6) Savas, P.; Virassamy, B.; Ye, C.; Salim, A.; Mintoff, C. P.; Caramia, F.; Salgado, R.; Byrne, D. J.; Teo, Z. L.; Dushyanthen, S.; Byrne, A.; Wein, L.; Luen, S. J.; Poliness, C.; Nightingale, S. S.; Skandarajah, A. S.; Gyorki, D. E.; Thornton, C. M.; Beavis, P. A.; Fox, S. B. Kathleen Cuningham Foundation Consortium for Research into Familial Breast, C., Darcy; P. K., SpeedT. P., Mackay, L. K. Neeson, P. J., Loi, Single-cell profiling of breast cancer T cells reveals a tissue-resident memory subset associated With improved prognosis. *Nat. Med.* **2018**, *24* (7), 986−993.
(7) Shae, D.; Becker, K. W.; Christov, P.; Yun, D. S.; Lytton-Jean, A. K. R.; Sevimli, S.; Ascano, M.; Kelley, M.; Johnson, D. B.; Balko, J. M.; Wilson, J. T. Endosomolytic polymersomes increase the activity of cyclic dinucleotide STING agonists to enhance cancer immunotherapy. *Nat. Nanotechnol* **2019**, *14* (3), 269−278.
(8) Wang, H.; Hu, S. Q.; Chen, X.; Shi, H. P.; Chen, C.; Sun, L. J.; Chen, Z. J. J. cGAS is essential for the antitumor effect of immune checkpoint blockade. *P Natl. Acad. Sci. USA* **2017**, *114* (7), 1637−1642.
(9) Woo, S. R.; Fuertes, M. B.; Corrales, L.; Spranger, S.; Furdyna, M. J.; Leung, M. Y.; Duggan, R.; Wang, Y.; Barber, G. N.; Fitzgerald, K. A.; Alegre, M. L.; Gajewski, T. F. STING-dependent cytosolic DNA sensing mediates innate immune recognition of immunogenic tumors. *Immunity* **2014**, *41* (5), 830−842.
(10) Deng, L. F.; Liang, H.; Xu, M.; Yang, X. M.; Burnette, B.; Arina, A.; Li, X. D.; Mauceri, H.; Beckett, M.; Darga, T.; Huang, X. N.; GajeWski, T. F.; Chen, Z. J. J.; Fu, Y. X.; Weichselbaum, R. R. STING-Dependent Cytosolic DNA Sensing Promotes Radiation-Induced Type I Interferon-Dependent Antitumor Immunity in Immunogenic Tumors. *Immunity* **2014**, *41* (5), 843−852.
(11) Corrales, L.; Mcwhirter, S. M.; Dubensky, T. W.; Gajewski, T. F. The host STING pathway at the interface of cancer and immunity. *J. Clin Invest* **2016**, *126* (7), 2404−2411.
(12) Spadaro, F.; Lapenta, C.; Donati, S.; Abalsamo, L.; Barnaba, V.; Belardelli, F.; Santini, S. M.; Ferrantini, M. IFN-alpha enhances cross-presentation in human dendritic cells by modulating antigen survival, endocytic routing, and processing. *Blood* **2012**, *119* (6), 1407−1417.
(13) Di Domizio, J.; Gulen, M. F.; Saidoune, F.; Thacker, V. V.; Yatim, A.; Sharma, K.; Nass, T.; Guenova, E.; Schaller, M.; Conrad, C.; Goepfert, C.; de Leval, L.; von Garnier, C.; BerezoWska, S.; Dubois, A.; Gilliet, M.; Ablasser, A. The cGAS-STING pathway drives type I IFN immunopathology in COVID-19. *Nature* **2022**, *603* (7899), 145−151.
(14) Vatner, R. E.; Janssen, E. M. STING, DCs and the link between innate and adaptive tumor immunity. *Mol. Immunol* **2019**, *110*, 13−23.
(15) Theofilopoulos, A. N.; Baccala, R.; Beutler, B.; Kono, D. H. Type I interferons (alpha/beta) in immunity and autoimmunity. *Annu. Rev. Immunol.* **2005**, *23*, 307−336.
(16) Shae, D.; Becker, K. W.; Christov, P.; Yun, D. S.; Lytton-Jean, A. K. R.; Sevimli, S.; Ascano, M.; Kelley, M.; Johnson, D. B.; Balko, J. M.; Wilson, J. T. Endosomolytic polymersomes increase the activity of cyclic dinucleotide STING agonists to enhance cancer immunotherapy. *Nat. Nanotechnol* **2019**, *14* (3), 269−278.
(17) wehbe, M.; Wang-Bishop, L.; Becker, K. W.; Shae, D.; Baljon, J. J.; He, X.; Christov, P.; Boyd, K. L.; Balko, J. M.; Wilson, J. T. Nanoparticle delivery improves the pharmacokinetic properties of cyclic dinucleotide STING agonists to open a therapeutic window for intravenous administration. *J. Controlled Release* **2021**, *330*, 1118−1129.
(18) Koshy, S. T.; Cheung, A. S.; Gu, L.; Graveline, A. R.; Mooney, D. J. Liposomal Delivery Enhances Immune Activation by STING Agonists for Cancer Immunotherapy. *Adv. Biosyst* **2017**, *1* (1−2), 1600013.
(19) Luo, M.; Wang, H.; Wang, Z.; Cai, H.; Lu, Z.; Li, Y.; Du, M.; Huang, G.; Wang, C.; Chen, X.; Porembka, M. R.; Lea, J.; Frankel, A. E.; Fu, Y. X.; Chen, Z. J.; Gao, J. A STING-activating nanovaccine for cancer immunotherapy. *Nat. Nanotechnol* **2017**, *12* (7), 648−654.
(20) Cheng, N.; Watkins-Schulz, R.; Junkins, R. D.; David, C. N.; Johnson, B. M.; Montgomery, S. A.; Peine, K. J.; Darr, D. B.; Yuan, H.; McKinnon, K. P.; Liu, Q.; Miao, L.; Huang, L.; Bachelder, E. M.; Ainslie, K. M.; Ting, J. P. A nanoparticle-incorporated STING activator enhances antitumor immunity in PD-L1-insensitive models of triple-negative breast cancer. *JCI Insight* **2018**, *3* (22), No. e120638.
(21) Dane, E. L.; Belessiotis-Richards, A.; Backlund, C.; Wang, J.; Hidaka, K.; Milling, L. E.; Bhagchandani, S.; Melo, M. B.; Wu, S.; Li, N.; Donahue, N.; Ni, K.; Ma, L.; Okaniwa, M.; Stevens, M. M.; Alexander-Katz, A.; Irvine, D. J. STING agonist delivery by tumour-penetrating PEG-lipid nanodiscs primes robust anticancer immunity. *Nat. Mater.* **2022**, *21* (6), 710−720.
(22) Reglero-Real, N.; Perez-Gutierrez, L.; Yoshimura, A.; Rolas, L.; Garrido-Mesa, J.; Barkaway, A.; Pickworth, C.; Saleeb, R. S.; Gonzalez-Nunez, M.; Austin-williams, S. N.; Cooper, D.; Vazquez-Martinez, L.; Fu, T.; De Rossi, G.; Golding, M.; Voisin, M. B.; Boulanger, C. M.; Kubota, Y.; Muller, W. A.; Tooze, S. A.; Nightingale, T. D.; Collinson, L.; Perretti, M.; Aksoy, E.; Nourshargh, S. Autophagy modulates endothelial junctions to restrain neutrophil diapedesis during inflammation. *Immunity* **2021**, *54* (9), 1989−2004.
(23) Ballesteros, I.; Rubio-Ponce, A.; Genua, M.; Lusito, E.; Kwok, I.; Fernandez-Calvo, G.; Khoyratty, T. E.; van Grinsven, E.; Gonzalez-Hernandez, S.; Nicolas-Avila, J. A.; Vicanolo, T.; Maccataio, A.; Benguria, A.; Li, J. L.; Adrover, J. M.; Aroca-Crevillen, A.; Quintana, J. A.; Martin-Salamanca, S.; Mayo, F.; Ascher, S.; Barbiera, G.; Soehnlein, O.; Gunzer, M.; Ginhoux, F.; Sanchez-Cabo, F.; Nistal-Villan, E.; Schulz, C.; Dopazo, A.; Reinhardt, C.; Udalova, I. A.; Ng, L. G.; Ostuni, R.; Hidalgo, A. Co-option of Neutrophil Fates by Tissue Environments. *Cell* **2020**, *183* (5), 1282−1297.
(24) Xue, J. W.; Zhao, Z. K.; Zhang, L.; Xue, L. J.; Shen, S. Y.; Wen, Y. J.; Wei, Z. Y.; Wang, L.; Kong, L. Y.; Sun, H. B.; Ping, Q. N.; Mo, R.; Zhang, C. Neutrophil-mediated anticancer drug delivery for suppression of postoperative malignant glioma recurrence. *Nat. Nanotechnol* **2017**, *12* (7), 692−700.
(25) Zhang, L.; Zhang, Y.; Xue, Y. N.; Wu, Y.; Wang, Q. Q.; Xue, L. J.; Su, Z. G.; Zhang, C. Transforming weakness into Strength: Photothermal-Therapy-Induced Inflammation Enhanced Cytopharmaceutical Chemotherapy as a Combination Anticancer Treatment. *Adv. Mater.* **2018**, *31* (5), No. e1805936.
(26) Ju, C. Y.; Wen, Y. J.; Zhang, L. P.; Wang, Q. Q.; Xue, L. J.; Shen, J.; Zhang, C. Neoadjuvant Chemotherapy Based on Abraxane/Human Neutrophils Cytopharmaceuticals with Radiotherapy for Gastric Cancer. *Small* **2019**, *15* (5), No. e1804191.
(27) Du, J.; Wang, C.; Chen, Y.; Zhong, L.; Liu, X.; Xue, L.; Zhang, Y.; Li, Y.; Li, X.; Tang, C.; Su, Z.; Zhang, C. Targeted downregulation of HIF-1alpha for restraining circulating tumor microemboli mediated metastasis. *J. control release* **2022**, *343*, 457−468.

https://doi.org/10.1021/acsnano.2c11764
ACS Nano 2023, 17, 1663−1680

(28) Zhang, Y.; Wang, C.; Li, W.; Tian, W.; Tang, C.; Xue, L.; Lin, Z.; Liu, G.; Liu, D.; Zhou, Y.; Wang, Q.; Wang, X.; Birnbaumer, L.; Yang, Y.; Li, X.; Ju, C.; Zhang, C. Neutrophil Cyto-Pharmaceuticals Suppressing Tumor Metastasis via Inhibiting Hypoxia-Inducible Factor-1alpha in Circulating Breast Cancer Cells. *Adv. healthc mater* **2022**, *11* (3), No. e2101761.
(29) Li, Y.; Hu, Q.; Li, W.; Liu, S.; Li, K.; Li, X.; Du, J.; Yu, Z.; Wang, C.; Zhang, C. Simultaneous blockage of contextual TGF-beta by cyto-pharmaceuticals to suppress breast cancer metastasis. *J. control release* **2021**, *336*, 40−53.
(30) Kolaczkowska, E.; Kubes, P. Neutrophil recruitment and function in health and inflammation. *Nat. Rev. Immunol* **2013**, *13* (3), 159−175.
(31) Ley, K.; Hoffman, H. M.; Kubes, P.; Cassatella, M. A.; Zychlinsky, A.; Hedrick, C. C.; Catz, S. D. Neutrophils: New insights and open questions. *Sci. Immunol* **2018**, *3* (30), No. eaat4579.
(32) Margraf, A.; Ley, K.; Zarbock, A. Neutrophil Recruitment: From Model Systems to Tissue-Specific Patterns. *Trends Immunol* **2019**, *40* (7), 613−634.
(33) Coffelt, S. B.; Wellenstein, M. D.; de Visser, K. E. Neutrophils in cancer: neutral no more. *Nat. Rev. Cancer* **2016**, *16* (7), 431−446.
(34) Kolaczkowska, E.; Kubes, P. Neutrophil recruitment and function in health and inflammation. *Nat. Rev. Immunol* **2013**, *13* (3), 159−175.
(35) Stephan, M. T.; Moon, J. J.; Um, S. H.; Bershteyn, A.; Irvine, D. J. Therapeutic cell engineering with surface-conjugated synthetic nanoparticles. *Nat. Med.* **2010**, *16* (9), 1035−1041.
(36) Gao, P.; Ascano, M.; Zillinger, T.; Wang, W.; Dai, P.; Serganov, A. A.; Gaffney, B. L.; Shuman, S.; Jones, R. A.; Deng, L.; Hartmann, G.; Barchet, W.; Tuschl, T.; Patel, D. J. Structure-function analysis of STING activation by c[G(2′,5′)pA(3′,5′)p] and targeting by antiviral DMXAA. *Cell* **2013**, *154* (4), 748−762.
(37) Stephan, M. T.; Stephan, S. B.; Bak, P.; Chen, J. Z.; Irvine, D. J. Synapse-directed delivery of immunomodulators using T-cell-conjugated nanoparticles. *Biomaterials* **2012**, *33* (23), 5776−5787.
(38) Sceneay, J.; Goreczny, G. J.; Wilson, K.; Morrow, S.; DeCristo, M. J.; Ubellacker, J. M.; Qin, Y. B.; Laszewski, T.; Stover, D. G.; Barrera, V.; Hutchinson, J. N.; Freedman, R. A.; Mittendorf, E. A.; McAllister, S. S. Interferon Signaling Is Diminished with Age and Is Associated with Immune Checkpoint Blockade Efficacy in Triple-Negative Breast Cancer. *Cancer Discov* **2019**, *9* (9), 1208−1227.
(39) Zhao, Y. H.; Zhang, W. N.; Huo, M. M.; Wang, P.; Liu, X. H.; Wang, Y.; Li, Y. N.; Zhou, Z. X.; Xu, N. Z.; Zhu, H. X. XBP1 regulates the protumoral function of tumor-associated macrophages in human colorectal cancer. *Signal Transduct Tar* **2021**, *6* (1), 357.
(40) Thery, C.; Duban, L.; Segura, E.; Veron, P.; Lantz, O.; Amigorena, S. Indirect activation of naive CD4(+) T cells by dendritic cell-derived exosomes. *Nat. Immunol* **2002**, *3* (12), 1156−1162.
(41) Mishalian, I.; Bayuh, R.; Levy, L.; Zolotarov, L.; Michaeli, J.; Fridlender, Z. G. Tumor-associated neutrophils (TAN) develop pro-tumorigenic properties during tumor progression. *Cancer Immunol Immunother* **2013**, *62* (11), 1745−1756.
(42) Jablonska, J.; Leschner, S.; Westphal, K.; Lienenklaus, S.; Weiss, S. Neutrophils responsive to endogenous IFN-beta regulate tumor angiogenesis and growth in a mouse tumor model. *J. Clin Invest* **2010**, *120* (4), 1151−1164.
(43) Singhal, S.; Bhojnagarwala, P. S.; O'Brien, S.; Moon, E. K.; Garfall, A. L.; Rao, A. S.; Quatromoni, J. G.; Stephen, T. L.; Litzky, L.; Deshpande, C.; Feldman, M. D.; Hancock, W. W.; Conejo-Garcia, J. R.; Albelda, S. M.; Eruslanov, E. B. Origin and Role of a Subset of Tumor-Associated Neutrophils with Antigen-Presenting Cell Features in Early-Stage Human Lung Cancer. *Cancer Cell* **2016**, *30* (1), 120−135.
(44) Buttari, B.; Profumo, E.; Caprari, P.; Massimi, S.; Sorrentino, F.; Maffei, L.; Gabbianelli, M.; Rigano, R. Phenotypical and functional abnormalities of circulating neutrophils in patients with beta-thalassemia. *Ann. Hematol* **2020**, *99* (10), 2265−2277.
(45) Zhu, J. W.; Doan, K.; Park, J.; Chau, A. H.; Zhang, H.; Lowell, C. A.; Weiss, A. Receptor-like Tyrosine Phosphatases CD45 and CD148 Have Distinct Functions in Chemoattractant-Mediated Neutrophil Migration and Response to S. aureus. *Immunity* **2011**, *35* (5), 757−769.
(46) Li, W.; Lu, L.; Lu, J.; Wang, X.; Yang, C.; Jin, J.; Wu, L.; Hong, X.; Li, F.; Cao, D.; Yang, Y.; Wu, M.; Su, B.; Cheng, J.; Yang, X.; Di, W.; Deng, L. cGAS-STING-mediated DNA sensing maintains CD8(+) T cell stemness and promotes antitumor T cell therapy. *Sci. Transl Med.* **2020**, *12* (549), No. eaay9013.
(47) Shao, D.; Zhang, F.; Chen, F. M.; Zheng, X.; Hu, H. Z.; Yang, C.; Tu, Z. X.; Wang, Z.; Chang, Z. M.; Lu, J. N.; Li, T. Y.; Zhang, Y.; Chen, L.; Leong, K. W.; Dong, W. F. Biomimetic Diselenide-Bridged Mesoporous Organosilica Nanoparticles as an X-ray-Responsive Biodegradable Carrier for Chemo-Immunotherapy. *Adv. Mater.* **2020**, *32* (50), No. e2004385.
(48) Chen, L.; Zhou, L. L.; Wang, C. H.; Han, Y.; Lu, Y. L.; Liu, J.; Hu, X. C.; Yao, T. M.; Lin, Y.; Liang, S. J.; Shi, S.; Dong, C. Y. Tumor-Targeted Drug and CpG Delivery System for Phototherapy and Docetaxel-Enhanced Immunotherapy With Polarization toward M1-Type Macrophages on Triple Negative Breast Cancers. *Adv. Mater.* **2019**, *31* (52), No. e1904997.

https://doi.org/10.1021/acsnano.2c11764
ACS Nano 2023, 17, 1663−1680